Journal of Building Engineering 114 (2025) 114208

Contents lists available at ScienceDirect

Journal of Building Engineering

journal homepage: www.elsevier.com/locate/jobe

Thermal performance of steel facade profiles: An experimental setup and self-shading assessment

Ricardo Lionar [a,*], David Kroll [a], Veronica Soebarto [a], Ehsan Sharifi [a], Marina Aburas [b]

[a] The University of Adelaide, SA, 5005, Australia
[b] BlueScope Building Components, Design Solution Group, Novar Gardens, SA, 5040, Australia

ARTICLE INFO

Keywords:
Energy demand
Building façade
Self-shading
Steel cladding
Heat gain reduction

ABSTRACT

The energy demand for heating and cooling in buildings is impacted by envelope design and construction. This study investigates how the profile shape, direction, orientation, and self-shading potential of common steel sheet profiles affect thermal performance, air flow and heat gain of the envelope. Three steel cladding profiles were tested under solar radiation in Adelaide's Mediterranean climate. Surface, cavity air, and internal space temperatures were recorded at 15-min intervals for different orientations and profile directions, while a fixed weather station monitored air temperature, humidity, wind speed, and solar radiation. The three steel sheet profiles are standing seam, corrugated, and interlocking. The Standing seam profile consistently exhibited the highest cavity temperature, with values exceeding that of the other profiles by up to 20 °C, indicating relatively poorer thermal performance under this setup. The Corrugated profile performed the best, particularly when oriented horizontally, reducing heat gain. The study also showed that airflow through natural convection within the cavity had a significant impact. Under more airtight conditions, the Interlocking profile, which lacked shading provided by the rib protrusion, exhibited higher cavity temperatures, with differences exceeding 14 °C compared to the other two profiles. This research provides valuable insights into the role of steel cladding profiles and self-shading in reducing cooling energy demand. It serves as a foundation for further exploration of steel sheet properties, rib depth, and profile design, supporting the development of energy-efficient building practices.

1. Introduction

Steel has been widely used in Australian construction since the 19th century, with its performance enhanced by coatings [1]. Steel cladding gained popularity during this period [2] and subsequently expanded both domestically and internationally [3]. In this context, steel cladding has gained momentum, due to its wide application on building envelopes, prefabrication potentials and being lightweight construction [4,5]. Cold Formed Steel (CFS) applied as roof and wall cladding is widely used in Australia to protect the critical elements of the building envelope due to its non-combustibility [6], strength-to-self-weight ratio, greater spanning capacity, and ease of installation [7]. CFS is frequently used in construction and applied in a broad range of contexts, including metal stud inner

* Corresponding author.
E-mail addresses: ricardo.lionar@adelaide.edu.au (R. Lionar), david.kroll@adelaide.edu.au (D. Kroll), veronica.soebarto@adelaide.edu.au (V. Soebarto), ehsan.sharifi@adelaide.edu.au (E. Sharifi), marina.aburas@bluescope.com (M. Aburas).

https://doi.org/10.1016/j.jobe.2025.114208
Received 19 May 2025; Received in revised form 15 September 2025; Accepted 26 September 2025
Available online 28 September 2025

walls and profiled roof sheeting. This versatility is made possible by efficient production techniques such as rolling and press-braking, which allow a high degree of form freedom [8].

Common steel cladding profiles in Australia include (1) corrugated sheets, often called “Open Profile Cladding”, which are widely used in residential and commercial construction due to their robustness and cost-effectiveness [9]; (2) standing seam profiles, often called "Closed Profile Cladding", used for high-end applications for their sleek aesthetic [4]; and (3) trapezoidal profiles, commonly applied in residential and industrial roof due to their structural efficiency and protection against wind uplift [10]. Not only do these profiles contribute structurally under the stressed skin concept where the sheet acts as a diaphragm to improve building stability [11], they also perform thermally through surface properties. High solar reflectivity and thermal emissivity of the external surface reduce solar heat gain [12] while surface coatings and roughness significantly influence heat transfer [13–15]. For example, Joudi et al. [9] found that high total solar reflectance (TSR) of exterior claddings can substantially reduce cooling demand, while low-emissivity interior surfaces limit heat radiated into indoor air. Light-coloured or reflective coatings have been reported to reduce peak roof surface temperatures [16,17], where studies by Levinson et al. [18] reported reduction of up to 14 K and ceiling heat flux by 21 %.

In addition to surface coatings and material properties, the geometry of cladding itself can provide self-shading, where parts of the sheet shade other areas and reduce solar heat gain. Self-shading has been shown to lower cooling demand by decreasing the amount of solar irradiation reaching building surfaces, without requiring additional materials or energy input [19]. While previous studies on self-shading focused primarily on building-scale morphology or glazed surfaces, there is limited research at the component level for opaque materials, particularly metallic claddings like steel [19]. Further, steel and metallic materials have been extensively studied for a variety of properties, including structural behaviour under corrosion [20], material classification and identification [21], hydrogen-induced damage monitoring [22], and property prediction using machine learning [23–25]. However, relatively few studies have addressed the thermal performance of steel cladding profiles in building envelopes. This highlights a knowledge gap: the role of steel cladding profile geometry in passively modulating heat transfer remains poorly understood [19].

We hypothesised that different steel cladding profiles, depending on their geometry and orientation, produce varying self-shading effects, which influence surface, cavity, and internal temperatures. Therefore, this study aims to determine which steel cladding profiles and orientations provide the most self-shading benefits and examine the factors that influence their thermal performance. The insights gained are intended to guide smarter use of cladding geometry to improve the thermal performance of buildings and to inform future profile optimisation in steel cladding applications. Specifically, the objectives of the study are to: (1) observe the impact of the shading provided by the steel sheet profile to the surface temperature; (2) analyse the cavity temperature behind the steel cladding sheets as well as the internal temperature of the structure; (3) assess the correlation between the environmental variables (i.e., wind direction, wind speed, solar radiation), the cavity and the internal temperatures; and (4) determine which profile performs best in reducing heat gain. The experiments are set up to provide insights into the impact of different steel sheet profiles and directions with different façade orientations to the sun on the external heat gain of a structure clad with steel sheets.

Given their widespread use and contrasting geometrical features, Standing Seam, Corrugated, and Interlocking profiles were selected to investigate how rib geometry and orientation influence self-shading, cavity ventilation, and thermal performance. These specific profiles provide representative cases for industry practice while highlighting the role of geometry-driven heat transfer mechanisms.

The Mediterranean climate of Adelaide, South Australia, was selected as the study environment. This region is characterised by hot, dry summers with high solar loads and mild winters [26] and is classified as *Csa* in the Köppen climate system, conditions under which overheating risks are significant. Steel cladding profiles are widely used in such climates, making improvements in its thermal performance directly relevant to practice. Understanding how profile geometry and orientation influence heat transfer in these conditions can provide guidance for optimising cladding performance. Furthermore, the findings are transferable to other regions in the same climate classification or with comparable summer conditions, including parts of Europe, North America, and East Asia where heat

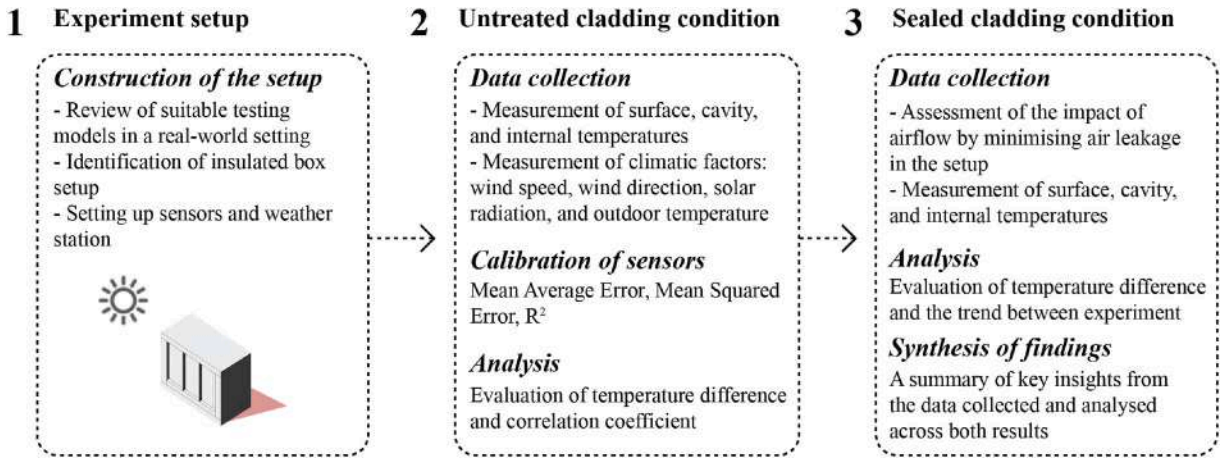

Fig. 1. Methodology used from the setup construction to the synthesis of findings.

waves are expected to increase in frequency and intensity across many continental regions [27]. This study specifically focuses on the thermal performance of insulated cladding profiles, in line with the Australian National Construction Code. Cavity temperatures are measured directly behind the steel cladding to assess the effect of the profile without insulation, while internal temperatures capture the thermal impact transmitted through insulation. By evaluating both, the study quantifies the influence of different steel cladding profiles under uninsulated and insulated conditions, providing insights for optimising cladding design for energy-efficient building envelopes.

2. Methodology

This section discusses the experimental setup, including background justifications, and the data collection processes (Fig. 1). The first data collection represents a real-world façade cladding configuration in which natural cavity airflow is permitted. In contrast, the second data collection was designed to isolate the effect of self-shading by sealing the cladding gaps, thereby limiting the airflow and reducing the convective heat transfer induced by solar radiation. Prior studies have demonstrated that solar radiation enhances cavity airflow through natural convection [28,29], while research by Hendawitharana et al. [30] indicates that sealing wall edges effectively controls this airflow. This approach facilitates a clearer assessment of the influence of self-shading on the façade's thermal performance.

2.1. Experimental setup

Several experimental setups have been used in previous studies to investigate the thermal performance of building materials, such as small timber-framed structures incorporating aerogel blankets [31] and insulated boxes with various wall assemblies [32]. The majority of these setups are referred to as hot boxes, typically equipped with an artificial heat source to measure heat flow across building components [33,34]. Among the identified studies, two of the most relevant test box setups are shown in Table 1. This research builds on those designs by employing a passive, insulated test box without an active heat source, relying instead on solar radiation to assess the thermal behaviour of steel cladding profiles. While traditional hot box systems can be costly, non-portable, and sensitive to the tested material's properties, recent studies have proposed more accessible alternatives. The present setup adopts key principles from previous designs while offering a practical and scalable approach for outdoor experimentation.

Table 1 presents two studies relevant to the aims of this research, both involving a setup with one surface exposed to external conditions. Chang et al. [35] constructed a compact 300 mm × 250 mm box to examine the thermal characteristics of glass with an insulating coating. However, the study lacks detailed information about the box's construction and materials. Conversely, Barbaresi et al. [33] used a larger insulated box to investigate the behaviour of materials exposed to external environments. Their setup combined Oriented Strand Board (OSB) and Expanded Polystyrene (EPS) to insulate the test chamber.

Taking into account the size and materials of the study and conventional construction standards in Australia, a new insulated box design was developed based on the work by Barbaresi et al. [33], incorporating several modifications as outlined below.

a) The dimensions of the insulated box were slightly reduced to 762 mm × 922 mm x 450 mm, allowing for easier mobility and handling during the experiment.
b) No additional apparatus such as a heat source or small fan was included to distribute heat inside the box. The focus of the study is on the heat generated from solar radiation.
c) The new design incorporates a thicker EPS (Expanded Polystyrene) insulation to comply with the minimum wall R-value for wall of class 5 commercial building in Climate zone 5 (R-value 1.4) [36] and mimics a typical light-weight steel cladding total R-value in Adelaide climate consisting of sarking, top hats, and Earthwool wall batt.
d) The hot box test is treated as a passive test that relies on solar radiation, with no artificial heating, cooling, or ventilation applied [37].

Small-scale boxes were used to provide controlled, reproducible measurements of cavity and internal air temperatures for validation-oriented purposes. These models cannot perfectly replicate all physical phenomena of full-scale buildings, particularly absolute magnitudes of convective and radiative heat transfer [38], but they allow consistent relative comparisons between different profiles and orientations under the same weather condition. Using sub-scale boxes enables multiple profiles to be tested simultaneously under identical environmental conditions, which would be difficult with full-scale constructions [39]. Some scale effects and time-dependent phenomena inevitably influence results [40], but these can be accounted for in the interpretation of the results, making this approach suitable for controlled comparative analysis and for generating data to calibrate or validate simulation models [38].

By implementing these modifications, the study developed a new insulated box design, which will later be used to calibrate the simulation of the steel cladding under solar radiation. The insulated box used Expanded Polystyrene (EPS) sheets (M Grade, 75 mm, R-value 1.99 m^2K/W) and Marine Plywood (AA Grade, 6 mm, R-value 0.05 m^2K/W). Three boxes were constructed, each featuring a distinct steel cladding profile with at least two modules. While low-cost test boxes often incorporate an active heat source to control and accelerate heat flow measurement, the present study employs a passive, solar-only setup. This approach allows the experiment to capture the thermal behaviour of steel cladding profiles under realistic environmental conditions, reflecting actual sun exposure, wind, and ambient temperature variations. Although solar simulators provide stable and controllable irradiance, spectrum, and uniformity for laboratory experiments [41,42], they cannot fully replicate the geometric characteristics of sunlight or the complex variability of

Table 1
Low-cost test box setup examples.

Author	Size	Standards	Intention	Instrumentation	Simulation method used	Hot and cold chamber	Layers of box (out to in)	Material being tested	Air tightness measurement	Image
Chang et al. [35]	30 × 25 × 12 cm	×	Real room is considered too big	1.500W halogen lamp as solar radiation 2.60W lamp as the room heat source 3. T-type thermocouple 4. Fan (forced ventilation)	×	×	1. Plywood (8 mm)	3 mm glass	×	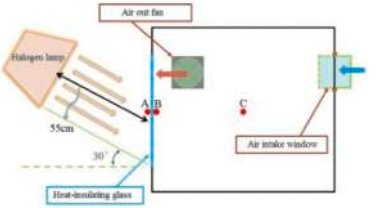
Barbaresi et al. [33]	100 × 100 × 100 cm	ISO 8301 EN ISO 8990 ISO 9869 ISO 7345	To build a smaller and affordable Hot Box to be used for experiments	1. Axial AC Fan 220VAC 2. Heater 1000W, 220V 3. Arduino with 2 relays, 1 display, 1 RTC clock, 6 DHT22 Temperature sensors	×	×	1. Expanded polystyrene (80 mm) 2. Oriented strand boards (18 mm)	1. Expanded polystyrene (80 mm) 2. Oriented strand boards (18 mm)	Thermoplastic adhesive. Thermal bridges are still detected through thermal cameras. Applied sensors far from the thermal bridges according to ISO 9869–2:2018	

outdoor solar irradiance caused by atmospheric, temporal, and climatic factors [43,44]. Using real sunlight, despite its variability and the challenges in measurement, ensures that the results reflect true outdoor conditions, including changes in angle of incidence, irradiance intensity, and spectral distribution, which are critical for assessing the actual performance of building materials.

To test a conservative case with higher heat absorption, three standard profiles: Standing Seam (SS), Corrugation (CR), and Interlocking (IL) were coated in a dark grey finish with a solar absorptivity of 0.73 - representing darker colours that are known to retain more heat and typically result in worse thermal performance. The cladding had an emissivity of 0.87 and a Total Solar Reflectance (TSR) of 0.27. The overall construction of the box, along with the cavity and internal zone, is presented in Figs. 2 and 3. The cavity temperature measured the effect of the cladding profile without insulation, while the internal temperature provided insights into how the insulation influenced the overall thermal performance of the building envelope.

The experimental site at The University of Adelaide's Waite Campus was selected due to its suitability for continuous monitoring and controlled placement of the test boxes, with details provided in Table 2. The experiment was conducted during the summer and early autumn months (January–April 2024), a period characterised by high solar exposure and elevated daytime temperatures, with maximum air temperatures exceeding 42 °C and global horizontal irradiance (GHI) reaching over 1075 W/m^2. These conditions represent the peak thermal stress typically experienced by steel cladding in Adelaide's hot, dry summer climate in Australian Climate Zone 5 [36], ensuring that the data captures the upper range of potential thermal loads. Predominant south-west winds and minimal

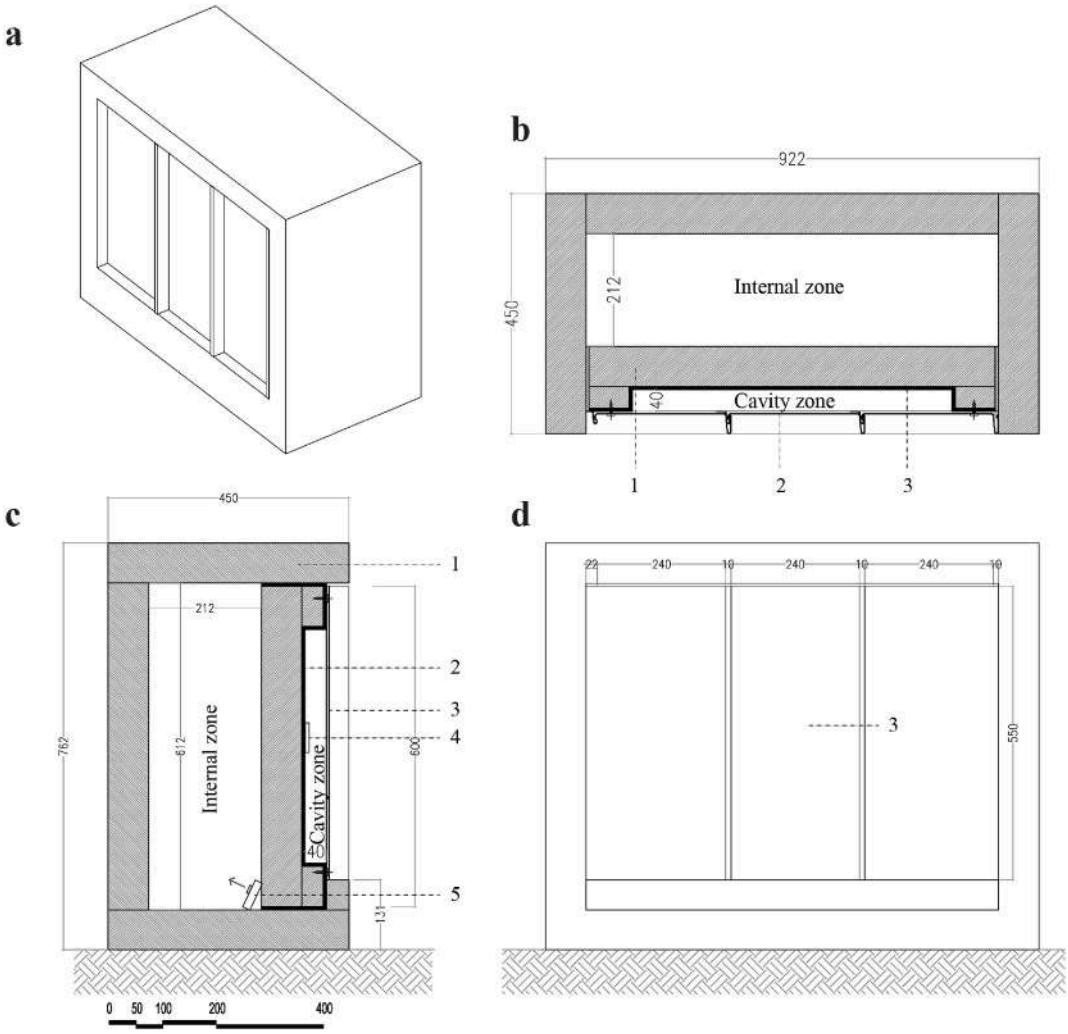

Fig. 2. Axonometry (a), horizontal section (b), vertical section (c), and front elevation (d) of the box.

Fig. 3. Assembly after the steel cladding is attached, along with the weather station.

Table 2
Experimental equipment, sensor specifications, and site conditions for thermal performance testing of steel cladding profiles.

Equipment	Model/Sensor	Measured Parameter	Accuracy	Placement/Notes
Data Loggers	HOBO MX2301A	Internal temperature	±0.2 °C (0–70 °C), ±0.25 °C outside	Inside box; see Fig. 2C
	HOBO MX2303	Surface/cavity temperature	±0.2 °C (0–70 °C), ±0.25 °C outside	Surface and cavity sensor locations (refer to Fig. 7)
	HOBO U12	Surface/cavity temperature	±0.35 °C (0–50 °C)	Surface and cavity sensor locations (refer to Fig. 7)
Adhesive	Thermally conductive tape	Securing sensors	Thermal conductivity 1.6 W/m·K	Ensures accurate surface heat transfer
Weather Station	HOBO U30	Temp, RH, wind, solar		Near the testing site
	Temp/RH Sensor with 2 m cable	Temp/RH	Temp ±0.2 °C, RH ±2.5 %–3.5 % (10 %–90 % RH)	Measures ambient conditions
	Davis® Smart Wind Sensor	Speed & direction	Speed ±1.1 m/s or 5 %, direction ±7°	Measures local wind
	Silicon Pyranometer	Solar irradiance	±10 W/m^2 or ±5 %, spectral 300–1100 nm	Measures Global Horizontal Irradiance
Location	Adelaide	Latitude −34.97, Longitude 138.64, Altitude 115 m	Free from obstructions; not public	Boxes levelled with timber pallets

cloud cover during this period further reflect realistic outdoor conditions. While the experiment was conducted at a single location, the fundamental physics governing heat gain, conduction, and dissipation in steel cladding remain the same across climates. Therefore, these results provide a reliable foundation for calibrating simulation models, which can subsequently be applied to different climate zones using appropriate weather files to assess performance under varied environmental conditions. The models were tested under two solar orientations: the north-facing orientation was selected because, in the Southern Hemisphere, it generally receives the most solar radiation over the course of the day, being equator-facing, while the west-facing orientation captures the higher-intensity afternoon sun when peak outdoor temperatures in Adelaide occur around 2–3 pm.

While ISO 9869–1:2014 states that the duration of monitoring should be at least 3–7 days [45], each configuration (with varying orientations and rib directions) was monitored for two weeks to ensure an adequate sample size for each iteration. The recording interval for the sensors used to gather the cavity, internal, surface, and outdoor temperature was 15 min to capture recurring patterns and significant deviations in environmental conditions over the course of the study [46]. The global horizontal irradiance (GHI), as well as wind speed and direction, were however recorded hourly using an on-site weather station, constrained by datalogger limitations. While the hourly recording may miss rapid changes such as transient cloud cover or short gusts of wind, it is considered sufficient for identifying overall trends in solar and wind conditions across the 2–3 weeks of the monitoring period. Since the primary analysis focuses on relative thermal responses between cladding profiles, the hourly weather data provide adequate accuracy for correlation with external drivers, while the higher-resolution 15-min temperature data ensure that short-term variations in thermal behaviour were still captured.

During the monitored period, a peak GHI of 1104 W/m^2 was recorded, while the wind speeds reached up to 7.7 m/s. The highest wind speeds occurred in the afternoon, and the wind direction was predominantly from the south-west, consistent with the prevailing wind patterns in Adelaide during summer and early autumn.

To account for potential convective losses through gaps or imperfections in the boxes, the experiment included a comparison between unsealed and sealed conditions. In the sealed configuration, grill mask tape was applied to the perimeter of the cladding

profile to reduce air leakage, while the unsealed configuration allowed small, uncontrolled airflow, mimicking real-world construction imperfections [4]. This approach enabled observation of the effect of sealing on cavity temperatures, while acknowledging that exact airflow rates within the small cavities were not measured.

To ensure all temperature sensor readings are consistent, during the sensor calibration process, all sensors were placed inside an insulated box made from polypropylene plastic to measure the air temperature. A factory-calibrated Kestrel air temperature sensor, with calibration standards traceable to the National Institute of Standards and Technology (NIST), was also used, with a recording interval of 30 min. The calibration methods were evaluated based on the Mean Average Error (MAE), Mean Squared Error (MSE), the mean of the Kestrel sensor reading, and the correlation coefficient squared R^2. The value for MAE indicates that the predictions were very close to the actual temperature values produced by the calibrated Kestrel sensor (0.05–0.08). Similarly, the MSE values for all sensors indicate that the errors after calibration were quite small (<0.01). The R^2 values are close to 1 (>0.995), indicating an excellent fit of the regression model to the data. Additionally, while the tolerance level according to NIST is 0.5°C [47], the error in the outcome after calibration falls within this tolerance range. While this calibration procedure ensures high precision, small systematic errors inherent to the sensors may remain, and the propagation of these uncertainties could influence derived temperature differences and

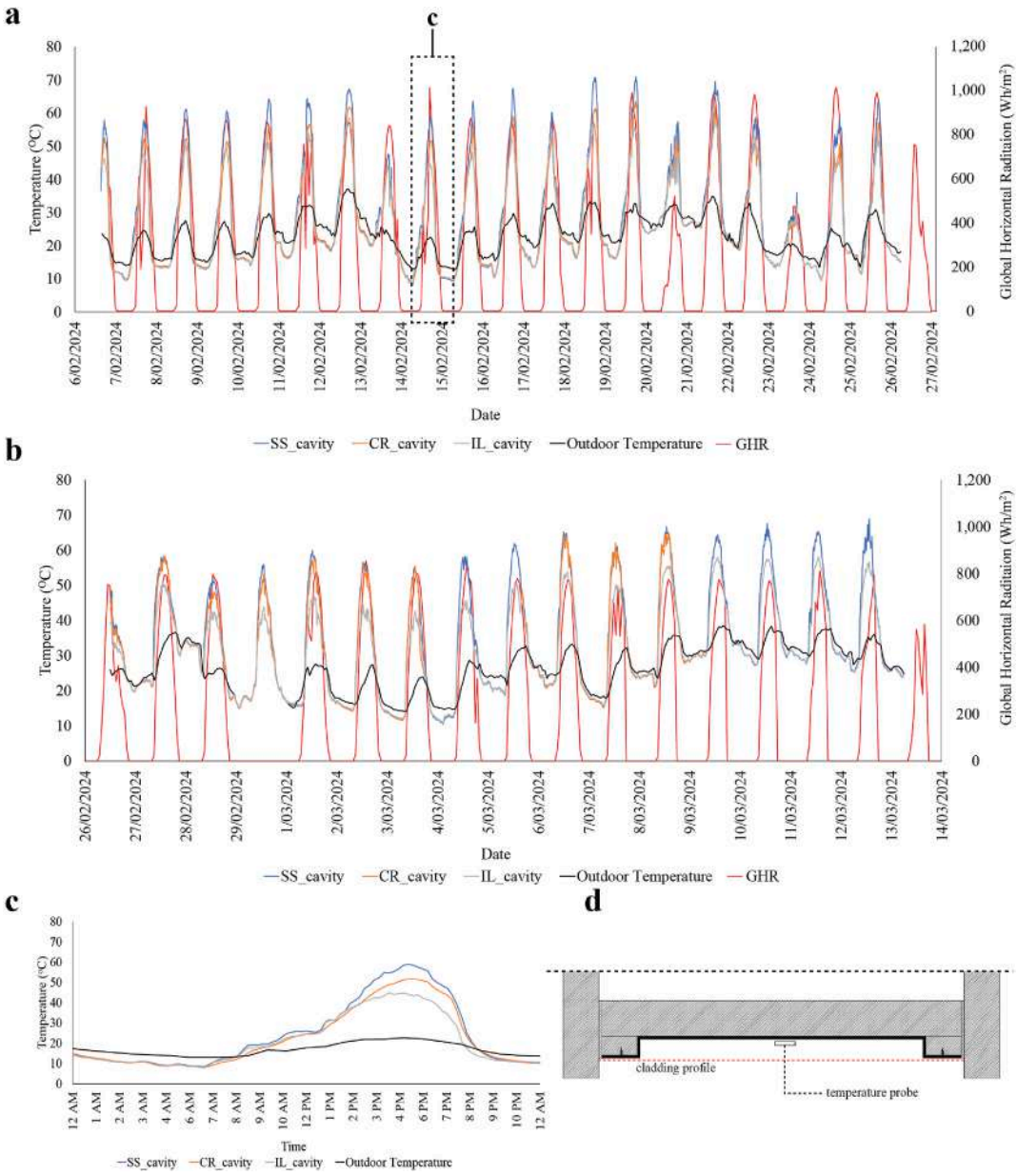

Fig. 4. Comparison of cavity temperatures at different measurement points: (a) west orientation with vertical ribs; (b) north orientation with vertical ribs; (c) representative data from 14 February for the west orientation; (d) measurement point locations.

trends. Additionally, the calibration was conducted under controlled indoor conditions, which differ from the outdoor experimental environment; thus, site-specific factors such as wind, direct sunlight, or local shading may introduce minor deviations in sensor response during the actual measurements. Overall, these considerations highlight that while the calibration provides a reliable baseline, the reported temperatures should be interpreted with these uncertainties in mind.

3. Results

3.1. Thermal performance of each profile

Fig. 4 shows the cavity temperatures behind the three different steel sheet profiles with two different rib directions (vertical and horizontal) and two orientations to the sun (north and west). The minimum temperature difference of 0 °C generally occurred at night (around 12 a.m.–3 a.m.), while the timing of the maximum temperature, which could reach more than 20 °C depended on the orientation—around 1 p.m.–3 p.m. for north-oriented cladding and 5 p.m.–7 p.m. for west-oriented cladding.

In a westward orientation with vertical ribs, SS (Standing Seam) profile exhibited the highest cavity temperature, reaching around 70 °C with a peak time at ~18:00 and a mean diurnal amplitude of ~45 °C, indicating a pronounced temperature swing (Fig. 4a). The CR (Corrugated) profile reached a maximum of ~64 °C (~17:45 peak, amplitude ~38 °C), while IL (Interlocking) profile remained the coolest (~59 °C, peak ~16:30, amplitude ~35 °C). The hours >2 °C above the coolest were 188 h for SS, 76 h for CR, and 22 h for IL, showing that SS retained higher temperatures for longer during the day, as shown in Table 3.

In the north orientation, SS profile and CR profile exhibited relatively similar cavity temperatures (Fig. 4b). Standing Seam consistently maintained a slightly higher cavity temperature compared to the Corrugated, with a difference of around 2 °C starting from 9 a.m. This temperature difference became more pronounced between 3 p.m. and 6 p.m. In contrast, the Interlocking profile consistently exhibited the lowest cavity temperature throughout the day. While it started with a temperature close to the other profiles in the morning, the temperature difference gradually widened to more than 15 °C by the afternoon (around 6 p.m.–8 p.m.). The SS profile had a daily mean of ~33 °C, CR ~31 °C, and IL ~31 °C; night means converged around 21–22 °C. The mean diurnal amplitude was highest for SS (~39 °C) and lowest for IL (~29 °C), while the persistence metric (hours >2 °C above the coolest) was 137 h, 72 h, and 2 h for SS, CR, and IL respectively, indicating that SS remained significantly hotter throughout the day.

With the profile rotated 90° to position the ribs horizontally, the trends become more pronounced compared to the vertical orientation (Fig. 5). The SS profile continued to show the highest cavity temperature, with the temperature difference peaking at more than 15 °C compared to the peak cavity temperatures of the other two profiles, around 1 p.m. However, during the night and into the morning, it exhibited the lowest surface temperature, approximately 3 °C lower than the CR Profile and less than 1 °C lower than the IL Profile. This lower temperature could be attributed to the SS profile outward-facing, fin-like ribs, which protrude more than the other profiles. These protrusions may have enhanced convective heat loss by increasing the surface area exposed to the cooler night air, thus allowing it to cool down more rapidly after sunset. The diurnal amplitude for horizontal SS was ~38 °C, CR ~24 °C, and IL ~31 °C, with hours >2 °C above the coolest at 78 h, 72 h, and 64 h, respectively, highlighting differences in heat retention and daytime temperature persistence.

In the west orientation, noticeable differences appear among the different profiles. The SS profile exhibited a significantly higher cavity temperature compared to the other profiles, with a temperature difference exceeding 20 °C compared to the CR profile and

Table 3
Summary of cavity temperature metrics for different steel sheet profiles (SS-standing seam, CR-Corrugated, IL-Interlocking), rib directions, and Facade orientations.

	Peak Temp (°C)	Peak Time	Daily Mean (°C)	Night Mean (00:00–06:00) (°C)	Mean Diurnal Amplitude (°C)[a]	Hours >2°C Above Coolest[b]
West vertical						
SS_cavity	70.94	February 19, 2024 18:00	28.92	16.85	44.69	187.8
CR_cavity	63.58	February 19, 2024 17:45	27.29	17	37.91	75.8
IL_cavity	58.67	February 21, 2024 16:30	26.54	16.77	34.77	22
North Vertical						
SS_cavity	68.8	March 12, 2024 13:30	33.27	22.39	38.95	137
CR_cavity	64.86	March 8, 2024 14:15	31.13	21.02	35.34	72
IL_cavity	58.1	March 11, 2024 13:15	30.77	22.52	28.95	2
North Horizontal						
SS_cavity	61.13	March 16, 2024 12:30	25.05	15.52	38.01	77.5
CR_cavity	44.12	March 24, 2024 13:00	21.04	14.13	23.69	72
IL_cavity	55.34	March 16, 2024 12:30	24.48	15.94	31.12	64
West Horizontal						
SS_cavity	71.9	March 29, 2024 17:30	21.58	12.39	40.16	91
CR_cavity	52.19	March 29, 2024 17:30	20.88	14.9	26.16	154
IL_cavity	60.59	March 29, 2024 18:00	21.1	13	32.75	90.5

[a] **Mean Diurnal Temperature:** Average of the daily maximum minus minimum cavity temperature, showing the typical day–night temperature swing.

[b] **Hours >2 °C Above Coolest:** Total number of hours in the period where a profile's cavity temperature is more than 2 °C higher than the coolest profile at the same time, indicating heat retention relative to other profiles.

approximately 9 °C compared to the IL profile. However, it is also observed that during the night, the CR profile showed a slightly higher temperature than the other profiles, with the temperature difference reaching more than 1.5 °C in the middle of the night. The mean night temperatures were 12–15 °C across profiles, while the mean diurnal amplitude was ~40 °C for SS, ~26 °C for CR, and ~33 °C for IL. The hours >2 °C above the coolest were 91 h for SS, 154 h for CR, and 91 h for IL, reflecting that CR retained heat longer into the night despite lower daytime peaks.

A comparison between the temperatures inside the model (box) with the different profiles, rib directions and orientations to the sun is presented in Fig. 6. With different orientation and ribs direction, the average internal temperature was found to range between 18 and 28 °C with the maximum temperature ranging between 37 and 46 °C and minimum temperature ranging between 8 and 11°C. On average, the air temperature inside the box remained relatively consistent across all profiles with a minimum temperature difference of 0 °C during the night and maximum temperature of more than 2 °C during the day.

Examining the diurnal patterns, the North horizontal orientation shows that SS and IL profiles reached peak temperatures around 13:30–13:45, with daily means of 21–21.4 °C, whereas CR profile peaked later around 14:15 and had a lower daily mean of 18.7 °C. The night-time mean temperatures were lowest for CR (12.8 °C), indicating faster cooling, while SS and IL retained slightly more warmth (16.5–16.7 °C). In contrast, the West horizontal orientation exhibits peak temperatures around 16:30–17:00 for all profiles, with CR maintaining the highest peak and largest persistence above the coolest profile (18.8 h), suggesting it retains heat more effectively overnight. SS and IL profiles had lower persistence values (0–2.2 h), indicating faster evening cooling. Notably, the CR Profile showed a slightly higher internal temperature when facing west and retained more heat overnight, aligning with its cavity temperature readings in the morning. This suggests that its corrugation might be more effective at retaining heat compared to the other profiles.

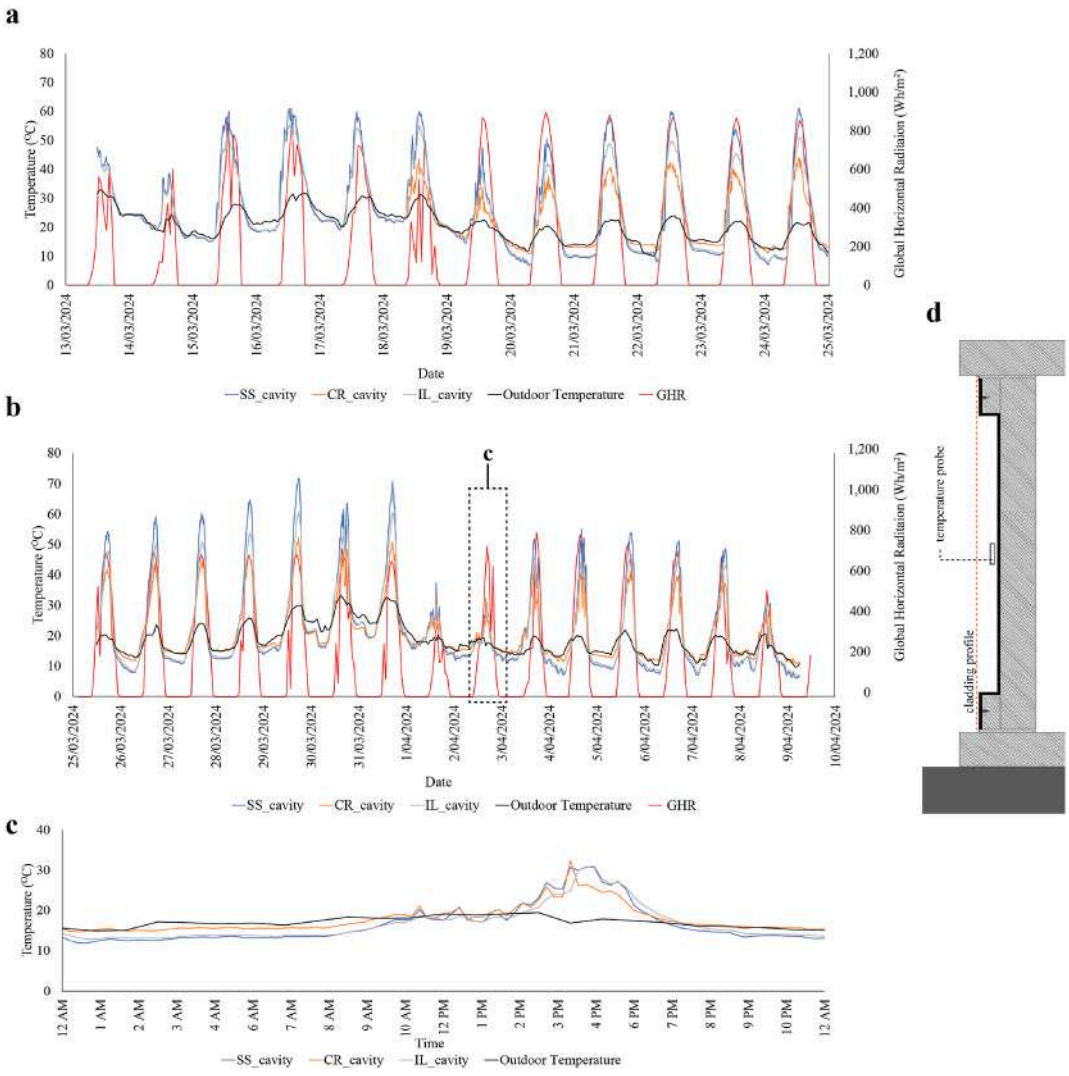

Fig. 5. Comparison of cavity temperatures at different measurement points: (a) north orientation with horizontal ribs; (b) west orientation with horizontal ribs; (c) representative data from 2 April; (d) measurement point locations.

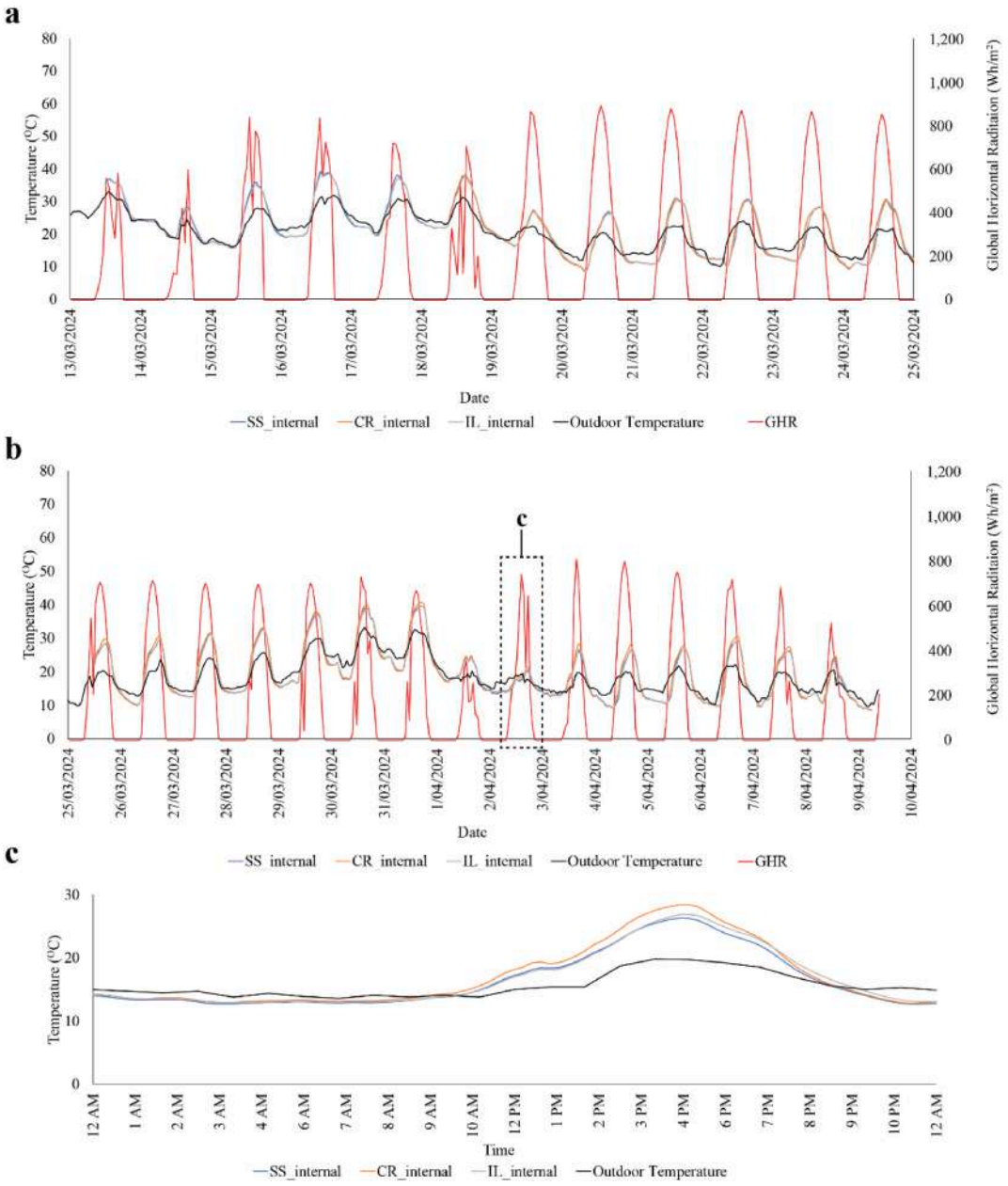

Fig. 6. Comparison of internal temperatures at different measurement points: (a) north orientation with horizontal ribs; (b) west orientation with horizontal ribs; (c) representative data from 2 April.

3.2. Standing seam profile surface temperature

To further understand the effect of the shaded area on the surface of the cladding, the surface temperature of each profile was measured. Fig. 7 shows the location of the surface temperature measuring points on each profile.

Overall, the average surface temperature of the ribs on the SS Profile (Standing seam) was lower compared to the other locations (Table 4), with the average temperature difference reaching nearly 2°C. This temperature difference occasionally exceeded 11 °C during the day.

In the west orientation with vertical ribs (Fig. 8), the surface on the northern part of the ribs reached a temperature 7°C higher than those on the southern part of the ribs by 5 p.m. Similarly, in the north orientation with vertical ribs (Fig. 8), the surface on the western part of the ribs shows elevated surface temperatures from 9 a.m. onwards as the sun started to impact the profile. By the afternoon, that surface registered lower surface temperatures than the other measurement points due to self-shading by the ribs.

With horizontally oriented ribs in SS, the north-facing surface located just above the ribs records the highest surface temperature,

while the temperature below the ribs shows the lowest, with a difference of nearly 5 °C (Fig. 9). During the day, the surface of the centre of the profile which had not received any shade from the ribs had the second highest temperature, while surfaces below the ribs remained 3–4 °C cooler due to shading. Similarly, when oriented west, the surface directly above the ribs facing the sun maintained the highest temperature, while the shaded surface beneath the ribs was up to 7 °C cooler than the other measured points.

3.3. Corrugated profile surface temperature

Fig. 7 shows the location of the surface temperature measurement points of the CR profile. Measurement point 1 was located on the valley part of the corrugation, while measurement points 2 and 3 were located on the sides of the crest, pointing to different orientations.

The average surface temperature reading overall showed a higher surface temperature of the valley, compared to the two points on the crest (Table 5). The maximum temperature difference would reach more than 12 °C. The surface temperatures of the crest, though pointing towards different directions, were quite similar with an average difference of less than 1°C.

Fig. 10 shows that the cavity temperature of the corrugated profile with vertical ribs reached a peak temperature of over 71 °C around 5 p.m., generally 5 °C higher than the surface temperatures. From noon to 4 p.m., the surface temperature of the eastern-facing crest was higher than that of the western-facing crest 3 by up to 7 °C. Later in the afternoon, the western-facing crest's surface temperature surpassed the eastern-facing crest as it received direct solar radiation until around 6 p.m. In the north orientation, the valley's temperature was consistently higher than the crest' between 9 a.m. and 3 p.m., with differences exceeding 4 °C compared to the east-facing crest, and over 7 °C compared to the west-facing crest. These disparities diminished after 3 p.m.

When oriented towards the north with horizontal ribs (Fig. 11), the surface temperatures on the valleys were relatively similar. From 9 a.m. to 3 p.m., the valley's surface temperature was consistently higher compared to the surface temperatures of the crest. The temperature difference between the valley and the upward-facing crest was around 1–2 °C, while the difference with the downward-facing crest exceeded 5 °C. In the west orientation (Fig. 11), the valley generally maintained a higher surface temperature in the afternoon, with a difference of more than 4 °C compared to the upward-facing crest and over 6 °C compared to the downward-facing crest due to the shading effect.

3.4. Interlocking profile surface temperature

Fig. 7 shows the location of the surface temperature measurement points on the IL profile. As opposed to having ribs, the IL profile has an inward-protruding part (recess).

Similar to the trend observed in the CR profile, the temperature of the recessed surface was consistently higher compared to that on the other measurement points, with an average temperature difference of 1.5 °C and a maximum difference exceeding 14 °C (Table 6).

In the west orientation with a vertical recess (Fig. 12a), all measurement points showed similar surface temperatures in the early morning and evening. By afternoon, the middle part of the cladding exhibited a higher surface temperature, exceeding that of the other locations by 2 °C. However, from 3 p.m. to 7 p.m., both surface temperatures in the recess surpassed the other, with differences over 4 °C.

Similarly, in the north orientation (Fig. 12b), the surface temperature in the recess reached its peak around 12 p.m., with differences diminishing after 4 p.m. The temperature on the outer surface was consistently lower, with differences exceeding 3 °C, especially around 9 a.m. and 3 p.m.

Similar to the trend with vertical recesses, in the north orientation with horizontal recesses (Fig. 13a), the surface temperature of the recess was higher than the other. In the west orientation (Fig. 13b), the recess temperature pointing towards the west was higher than the surface also located on the recess but pointed downward, by over 6 °C after 1 p.m., while the temperature of the outer surface

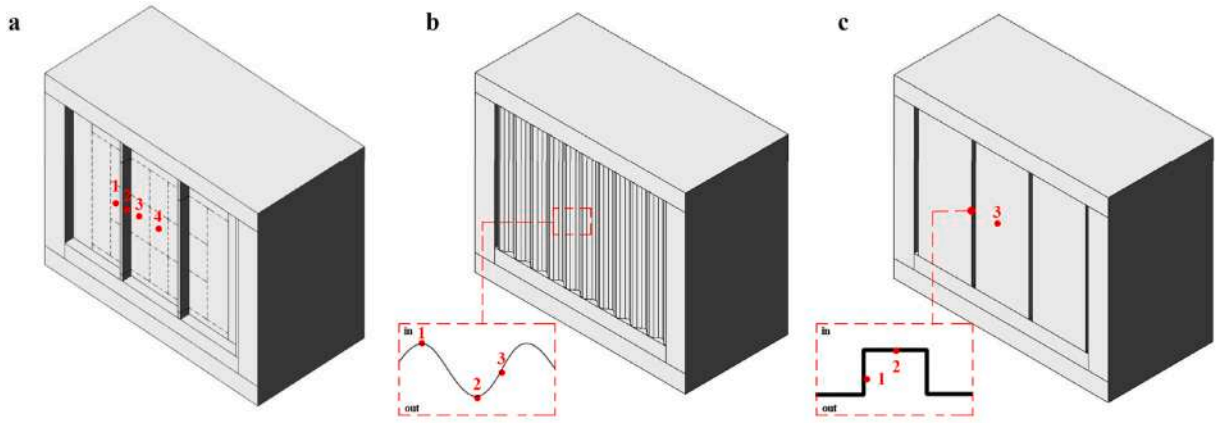

Fig. 7. Surface measurement points locations for SS (Standing seam) profile (a), CR (Corrugated) profile (b), and IL (Interlocking) profile (c).

Table 4
Comparison of surface temperature measurement points on the SS (Standing seam) profile.

Period	Orientation	Direction	Cladding type	Measurement points pair	Min Temp Difference (°C)	Max Temp Difference (°C)	Avg Temp Difference (°C)
6/02–26/02	West	Vertical	Standing seam	Point 1 - Point 2	0.00 (occurred during the night)	+10.91	+1.62
				Point 1 - Point 3		+6.21	+0.59
				Point 1 - Point 4		+5.76	+0.78
				Point 2 - Point 3		+9.52	−1.51
				Point 2 - Point 4		+7.72	−0.94
				Point 3 - Point 4		+7.25	+0.78
26/02–13/03	North	Vertical	Standing seam	Point 1 - Point 2	0.00 (occurred during the night)	+11.29	+1.92
				Point 1 - Point 3		+8.96	+1.16
				Point 1 - Point 4		−6.90	+0.93
				Point 2 - Point 3		+9.39	−1.37
				Point 2 - Point 4		+10.59	−1.20
				Point 3 - Point 4		+7.78	+0.99
18/03–25/03	North	Horizontal	Standing seam	Point 1 - Point 2	0.00 (occurred during the night)	+7.82	+1.25
				Point 1 - Point 3		+7.82	+1.23
				Point 1 - Point 4		+8.32	+0.90
				Point 2 - Point 3		+3.77	−0.56
				Point 2 - Point 4		+4.80	−0.54
				Point 3 - Point 4		+5.51	−0.62
25/03–09/24	West	Horizontal	Standing seam	Point 1 - Point 2	0.00 (occurred during the night)	+8.70	+1.20
				Point 1 - Point 3		+6.95	+0.79
				Point 1 - Point 4		+6.27	+0.66
				Point 2 - Point 3		+9.20	−0.96
				Point 2 - Point 4		−8.20	−0.85
				Point 3 - Point 4		+6.25	+0.61

+ Indicates the first profile has a higher temperature, - Indicates the first profile has a lower temperature.

remained lower than that on the recess, with differences exceeding 7 °C in the afternoon.

3.5. Effects of wind speed on temperature

Facade shape influences wind behaviour [48], which in turn affects thermal performance [49]. Therefore, to determine the effect of wind speed and direction on the observed temperature, a correlation analysis was conducted.

The correlation analysis reveals statistically significant ($p < 0.001$) but weak positive correlations between wind speed and temperature variables (surface, cavity, and internal), depending on the cladding orientation and rib/recess direction. Correlation significance varies with changing wind direction. To address this, data were filtered based on cladding orientation matching wind direction. For west-facing surfaces, wind directions with west components (West, Southwest, Northwest) are used, while for north-facing surfaces, north components (North, Northwest, Northeast) are selected.

When wind direction-matched datasets were analysed, stronger statistically significant correlations ($p < 0.001$) were observed (Fig. 14). For instance, in the Standing Seam profile, oriented west with vertical ribs, the correlation coefficient between wind speed and the surface temperature doubled (from <0.2 to around 0.5) when wind direction was considered, indicating a moderate association. Similarly, the correlation between wind speed and cavity temperature increased ($p < 0.001$) when the cladding was oriented towards the wind direction, a trend observed across all three profiles. However, overall, stronger correlations can be seen in the case of vertical orientation compared to the horizontal orientation, where correlations can be higher than 0.6 while the horizontal ribs on average, have only 0.2.

3.6. Isolating the effect of air infiltration

The result from the previous correlation might indicate the role of wind in influencing the cavity and internal temperature, which in turn indicates that there is air leakage on the attachment around the steel sheet on the box. To investigate the extent to which airflow influences the cavity temperature, airflow was restricted by applying grill mask tape around the perimeter of the steel cladding and sealing potential entry points around the perimeter of the cladding (Fig. 15). Testing was conducted with horizontal ribs oriented towards the west over a one-week period (11–18 November 2024). Temperature measurements, including surface, cavity, and internal temperatures, were recorded during this time.

For the surface temperature of each profile, the trend mirrored previous observations: the temperature of the ribs' surface in the SS profile exhibited lower temperatures than the temperature of the surfaces not being shaded by the ribs (with a maximum temperature difference of more than 10°C). For other profiles, the temperature of the surfaces on the recessed areas (or on the valley for the CR profile) showed higher temperatures (Table 7).

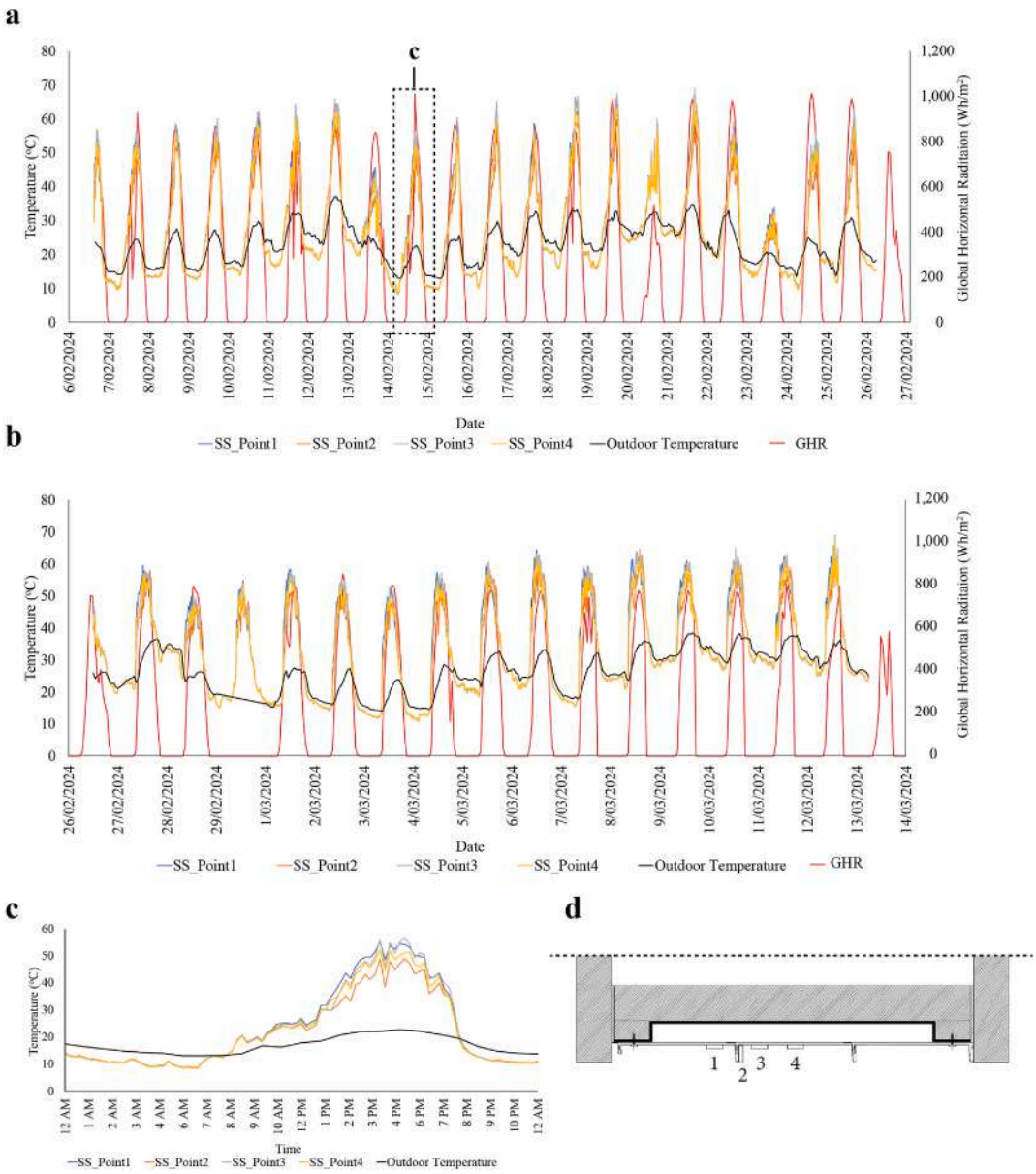

Fig. 8. Comparison of surface temperatures for the SS (Standing seam) profile at different measurement points: (a) west orientation with vertical ribs; (b) north orientation with vertical ribs; (c) representative data from 14 February for west orientation; (d) measurement point locations.

However, when examining the cavity temperature, the readings indicate that the SS profile had the lowest average temperature compared to the other two profiles. The IL profile, which lacks shaded surfaces, showed a higher cavity temperature, with a maximum difference of more than 14 °C compared to the SS profile. As for the internal temperature, the average temperature difference between profiles was also minimal (around 0.2 °C). However, maximum internal temperature was observed in the IL profile, which was more than 2 °C higher than the CR profile, mirroring the trend in the cavity temperature readings.

4. Discussion

4.1. Profile shape and its effect on cavity and internal temperature

This study highlights the significant influence of profile design, orientation, and rib positioning on cavity temperature performance, in conjunction with airflow. The observed timing of the minimum and maximum cavity temperature differences can be attributed to the variation in solar exposure throughout the day. North-facing cladding receives the most sunlight during midday, while west-facing cladding is exposed to stronger afternoon sun, causing peak temperatures to occur later in the day. At night, solar radiation is absent,

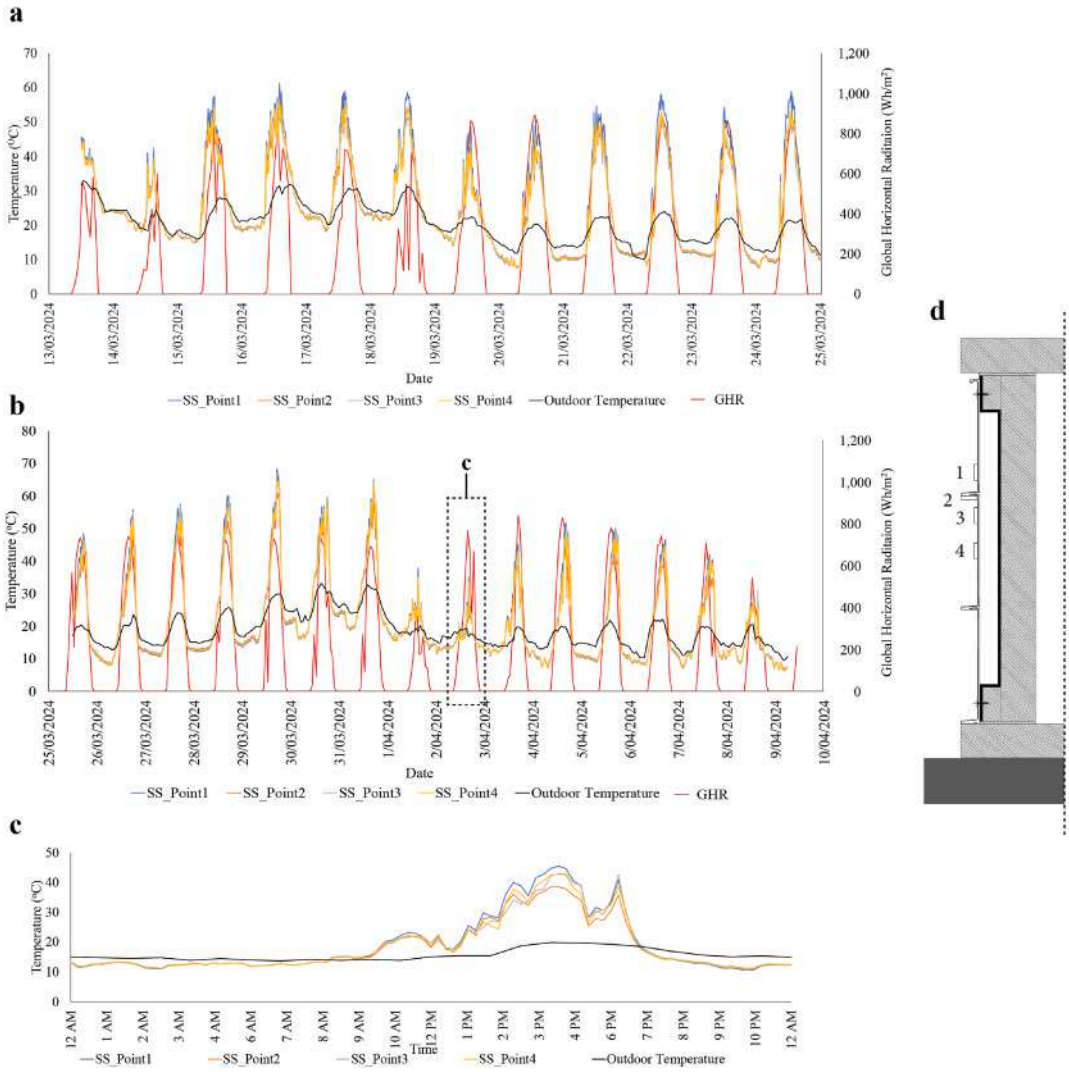

Fig. 9. Comparison of surface temperatures for the SS (Standing seam) profile at different measurement points: (a) north orientation with horizontal ribs; (b) west orientation with horizontal ribs; (c) representative data from 2 April for west orientation; (d) measurement point locations.

Table 5
Comparison of surface temperature measurement points on the CR (Corrugated) profile.

Period	Orientation	Direction	Measurement points pair	Min Temp Difference (°C)	Max Temp Difference (°C)	Avg Temp Difference (°C)
6/02–26/02	West	Vertical	Point 1- Point 2	0.00 (occurred during the night)	−6.06	+0.71
			Point 1- Point 3		+12.21	+1.22
			Point 2- Point 3		+10.84	+1.19
26/02–13/03	North	Vertical	Point 1- Point 2	0.00 (occurred during the night)	+8.43	+0.43
			Point 1- Point 3		+10.70	+0.83
			Point 2- Point 3		−11.17	+0.85
18/03–25/03	North	Horizontal	Point 1- Point 2	0.00 (occurred during the night)	+3.80	+0.45
			Point 1- Point 3		+12.19	+0.74
			Point 2- Point 3		−8.64	+0.65
25/03–09/24	West	Horizontal	Point 1- Point 2	0.01	−6.95	+0.91
			Point 1- Point 3	0.00	+15.86	+0.83
			Point 2- Point 3	0.01	+11.73	+0.93

+ Indicates the first profile has a higher temperature, - Indicates the first profile has a lower temperature.

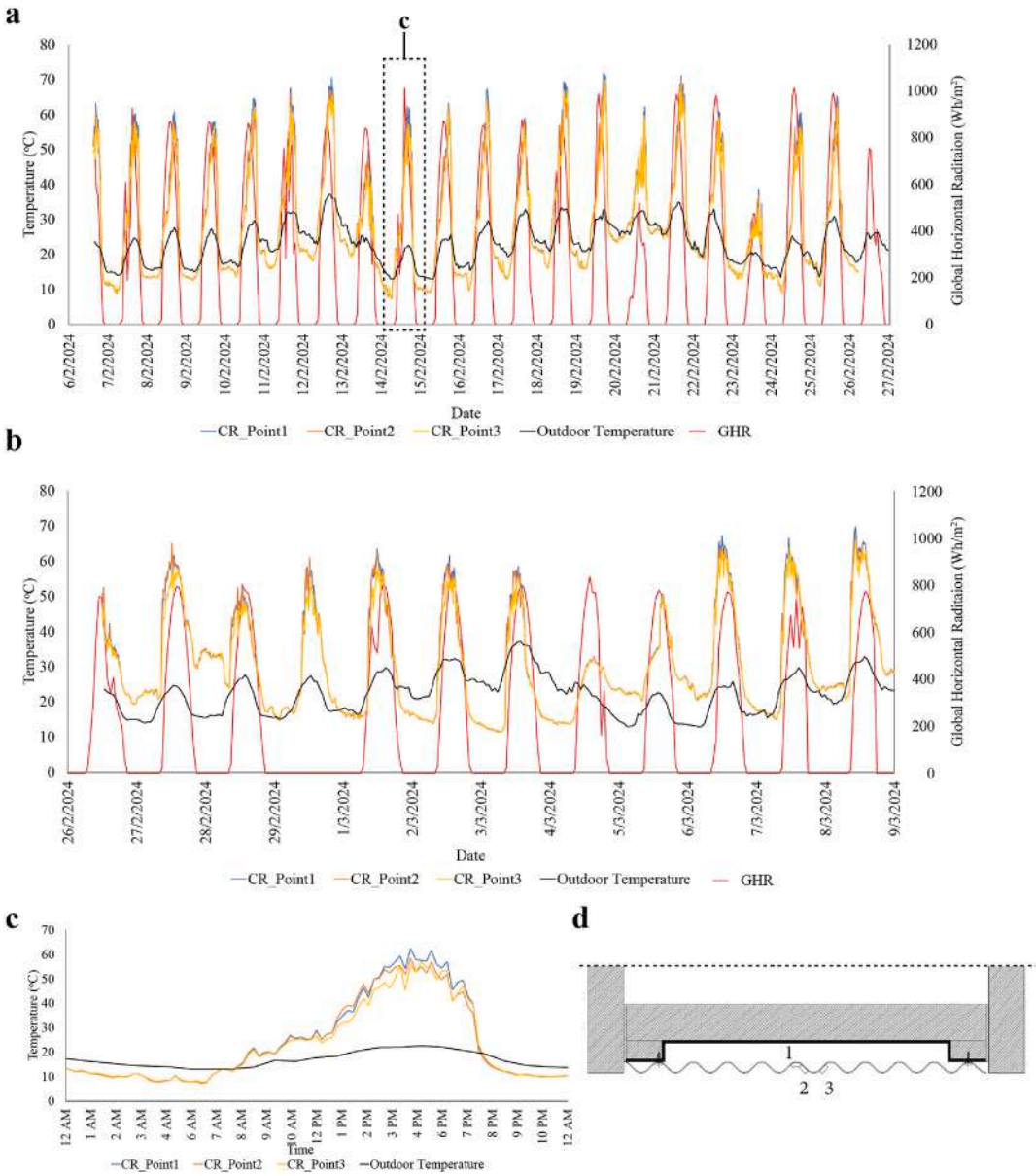

Fig. 10. Comparison of surface temperatures for the CR (Corrugated) profile at different measurement points: (a) west orientation with vertical ribs; (b) north orientation with vertical ribs; (c) representative data from 14 February for west orientation; (d) measurement point locations.

and all profiles cool to ambient levels, resulting in negligible temperature differences.

The faster nighttime cooling observed in the SS profile may be influenced by its geometric form. The fin-like ribs protrude outward by approximately 3.5 cm, which increases the profile's exposure to ambient air and may enhance convective cooling after sunset. This aligns with shading principles and fin array studies, where extended protrusions improve convective heat loss [50,51]. Increased surface exposure promotes faster convective heat loss because a larger surface area provides more contact with the surrounding air, increasing the rate at which heated air can be removed and replaced by cooler air [52,53]. This principle is central to convection, where heat is carried away from an object by the movement of air, with the rate of loss directly related to the amount of surface area available for this heat exchange [54].

In contrast, the interlocking profile's recessive design and the corrugated profile's smoother curves may reduce airflow turbulence and thus retain heat slightly longer into the night. This aligns with general thermal behaviour observed in previous studies, where smoother surfaces, such as the corrugated profile, reduce re-circulation zones and airflow turbulence, leading to less efficient mixing of the air and lower heat transfer from the surface [55]. In contrast, profiles with more pronounced ribs, like the standing seam, enhance turbulence, improving fluid-solid interaction and promoting more effective heat removal. Previous studies on natural convection in

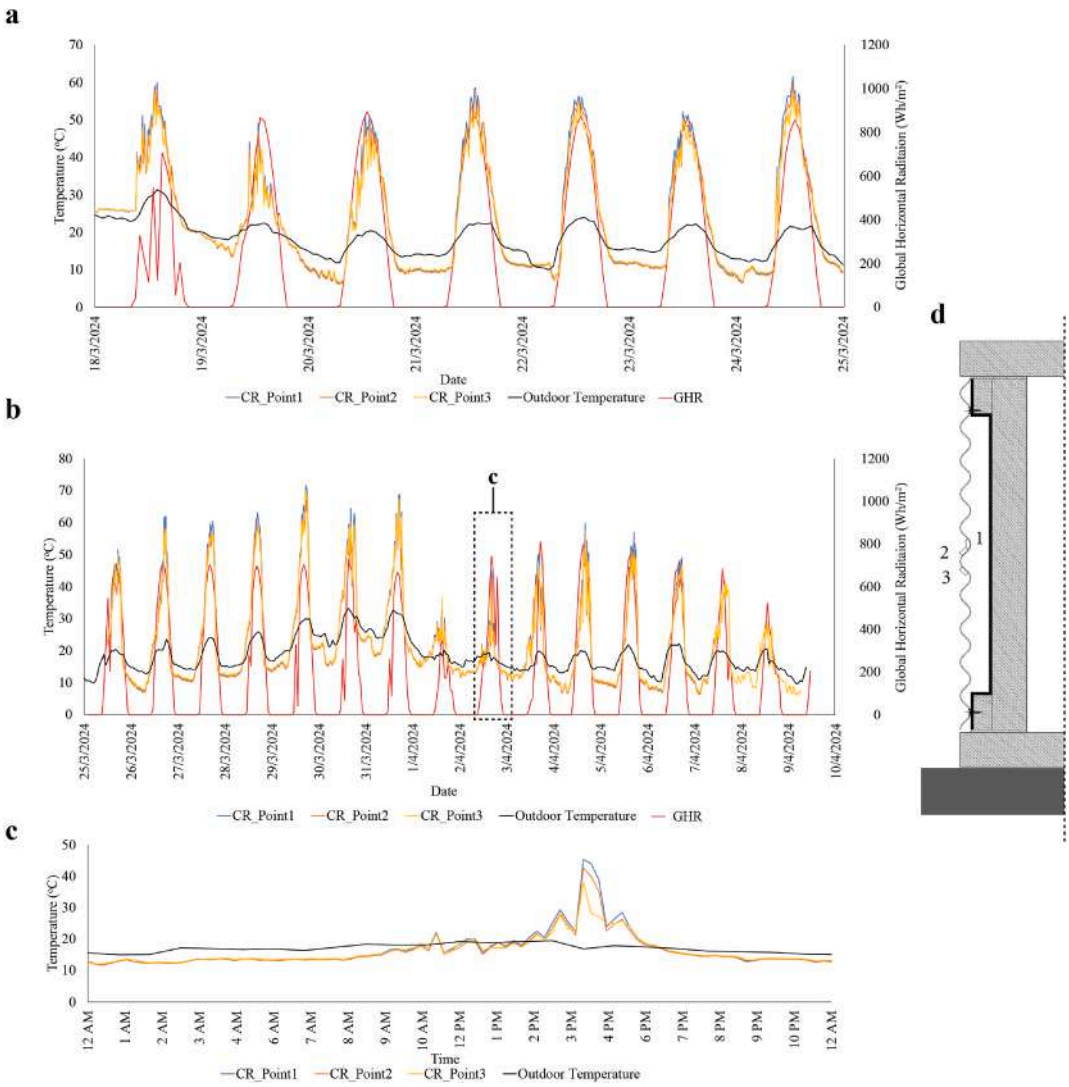

Fig. 11. Comparison of surface temperatures for the CR (Corrugated) profile at different measurement points: (a) north orientation with horizontal ribs; (b) west orientation with horizontal ribs; (c) representative data from 2 April for west orientation; (d) measurement point locations.

cavities indicate that laminar flow results in lower convective heat transfer, while turbulent flow enhances mixing and increases heat removal [56,57].

The results indicate that, under a common condition where no airtightness measures are specifically applied to the steel cladding, the standing seam profile exhibits a higher cavity temperature. On the other hand, the CR and IL profiles show different thermal behaviours depending on rib orientation, with CR being more effective when the ribs are positioned horizontally, and IL being more effective when the ribs are positioned vertically.

This finding may be attributed to the cavity size imposed by each of the profiles. When applied to the insulated box, the total cavity widths for the profiles were 44 mm, 62 mm, and 62 mm for the SS, CR, and IL profiles, respectively. Previous studies on cavity temperatures have shown that wider cavities or gaps tend to generate higher airflow rates and lower heat gains [58]. However, studies also reveal that beyond a certain threshold of cavity width, the ventilation rates started to decline [59,60]. This threshold is far wider than the common cavity depth for any standard airspace listed on BCA NCC (i.e., 70 mm for external wall cladding) [36].

The thermal performance observed in the CR profile, particularly the cooling effect associated with increased valley depth and denser corrugation, can be linked to self-shading characteristics. Zupan et al. [61] investigated how varying the amplitude and period of sinusoidal wrinkle patterns impacts surface self-shading and found that smaller periods and higher frequencies led to greater self-shading throughout the day, especially for west-facing orientations. These findings could be seen from the result of this study, where the CR profile, though having a similar valley depth to the IL profile's depth, with more ribs in the same wall area, provided more shading, thus resulting in lower cavity temperature compared to the IL profile.

The extended analysis of cavity and internal temperatures provides further insight into the diurnal behaviour of each profile. For

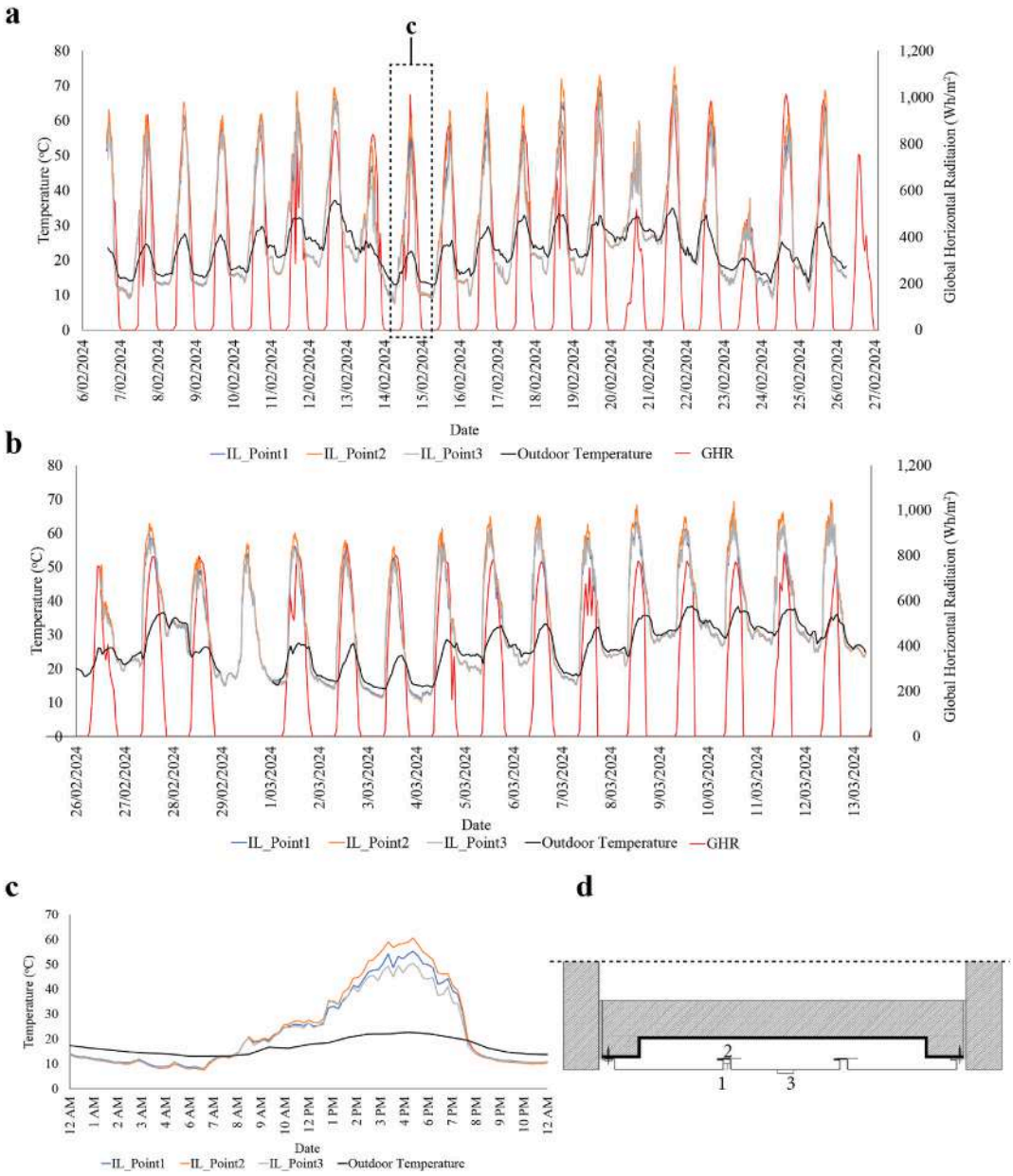

Fig. 12. Comparison of surface temperatures for the IL (Interlocking) profile at different measurement points: (a) west orientation with vertical ribs; (b) north orientation with vertical ribs; (c) representative data from 14 February for west orientation; (d) measurement point locations.

the North horizontal and West horizontal orientations, SS profiles consistently reached the highest peak cavity temperatures, with peak timing aligning with solar exposure (around 12:30–13:30 for north and 16:30–17:00 for west). The CR profile displayed higher internal temperatures during horizontal rib orientation and maintained greater persistence above the coolest profile overnight, particularly in the west-facing orientation (up to 18.8 h). The IL profile generally exhibited lower cavity and internal temperatures during the day but retained warmth moderately into the night, showing a smaller diurnal amplitude. These patterns demonstrate that rib configuration and orientation not only affect peak temperatures but also the daily mean, night-time retention, and thermal persistence of the cavity and internal air.

Although the internal air temperature in this setup did not reflect full-scale indoor conditions, the box provided a practical and affordable method to compare the thermal performance of different steel cladding profiles. The 75 mm EPS insulation was selected to approximate a typical R-value for the Adelaide climate, offering a consistent baseline for testing. While the setup lacked thermal mass and natural ventilation, it allowed for direct measurement of cavity temperatures and the effect of cladding on the insulated zone behind. The observed trends, when interpreted with fundamental heat transfer theory, provide a theoretical framework for

Table 6
Comparison of surface temperature measurement points on the IL (Interlocking) profile.

Period	Orientation	Direction	Measurement points pair	Min Temp Difference (°C)	Max Temp Difference (°C)	Avg Temp Difference (°C)
6/02–26/02	West	Vertical	Point 1- Point 2	0.00 (occurred during the night)	−8.70	−1.12
			Point 1- Point 3		+11.27	+0.85
			Point 2- Point 3		+14.83	+1.68
26/02–13/03	North	Vertical	Point 1- Point 2	0.00 (occurred during the night)	−4.44	−1.09
			Point 1- Point 3		−4.39	−0.58
			Point 2- Point 3		+7.23	+1.08
18/03–25/03	North	Horizontal	Point 1- Point 2	0.00 (occurred during the night)	−8.04	−1.31
			Point 1- Point 3		−4.13	+0.67
			Point 2- Point 3		+7.50	+1.02
25/03–09/24	West	Horizontal	Point 1- Point 2	0.00 (occurred during the night)	−8.04	−1.27
			Point 1- Point 3		−5.46	+0.75
			Point 2- Point 3		+8.39	+0.91

+ Indicates the first profile has a higher temperature, - Indicates the first profile has a lower temperature.

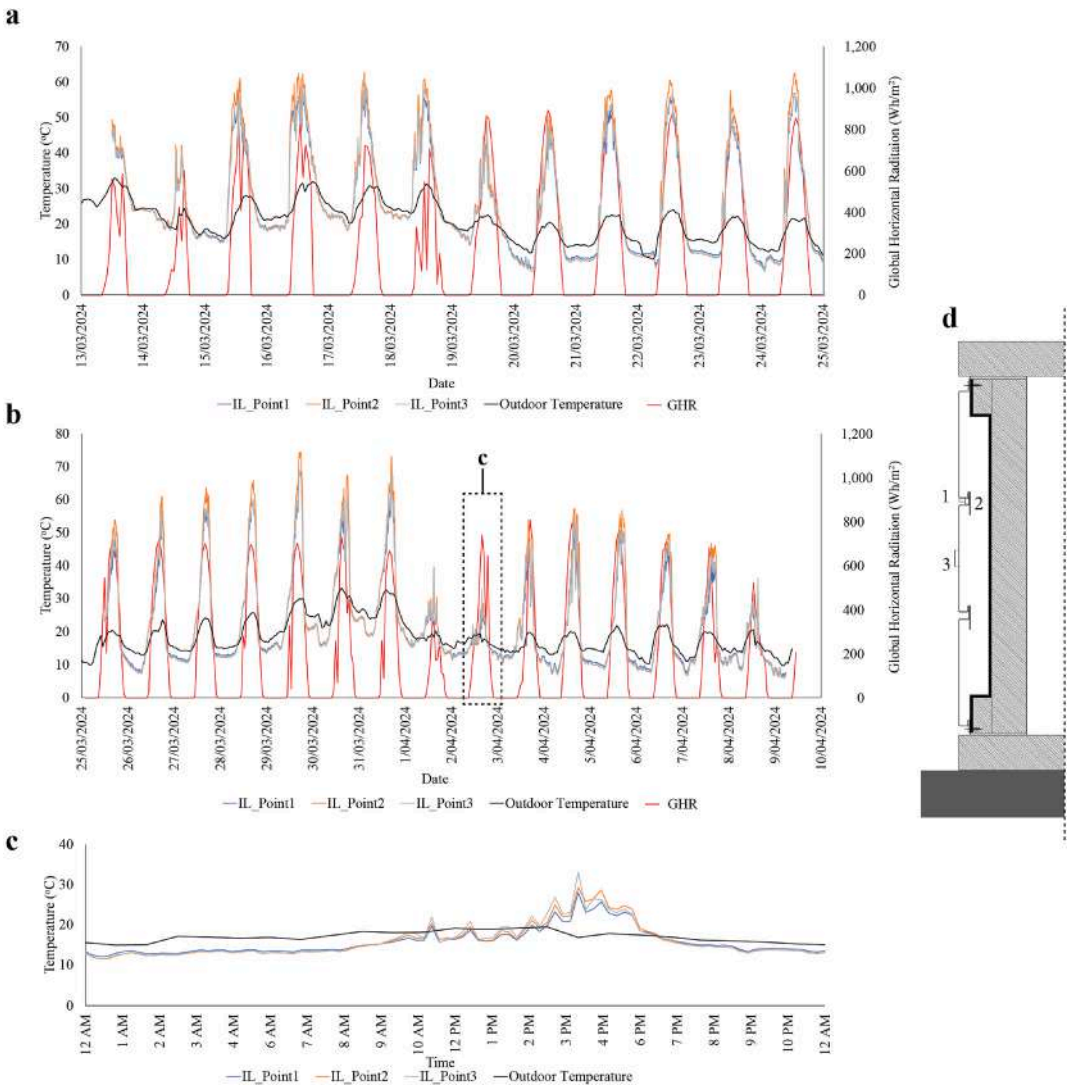

Fig. 13. Comparison of surface temperatures for the IL (Interlocking) profile at different measurement points: (a) north orientation with horizontal ribs; (b) west orientation with horizontal ribs; (c) representative data from 2 April for west orientation; (d) measurement point locations.

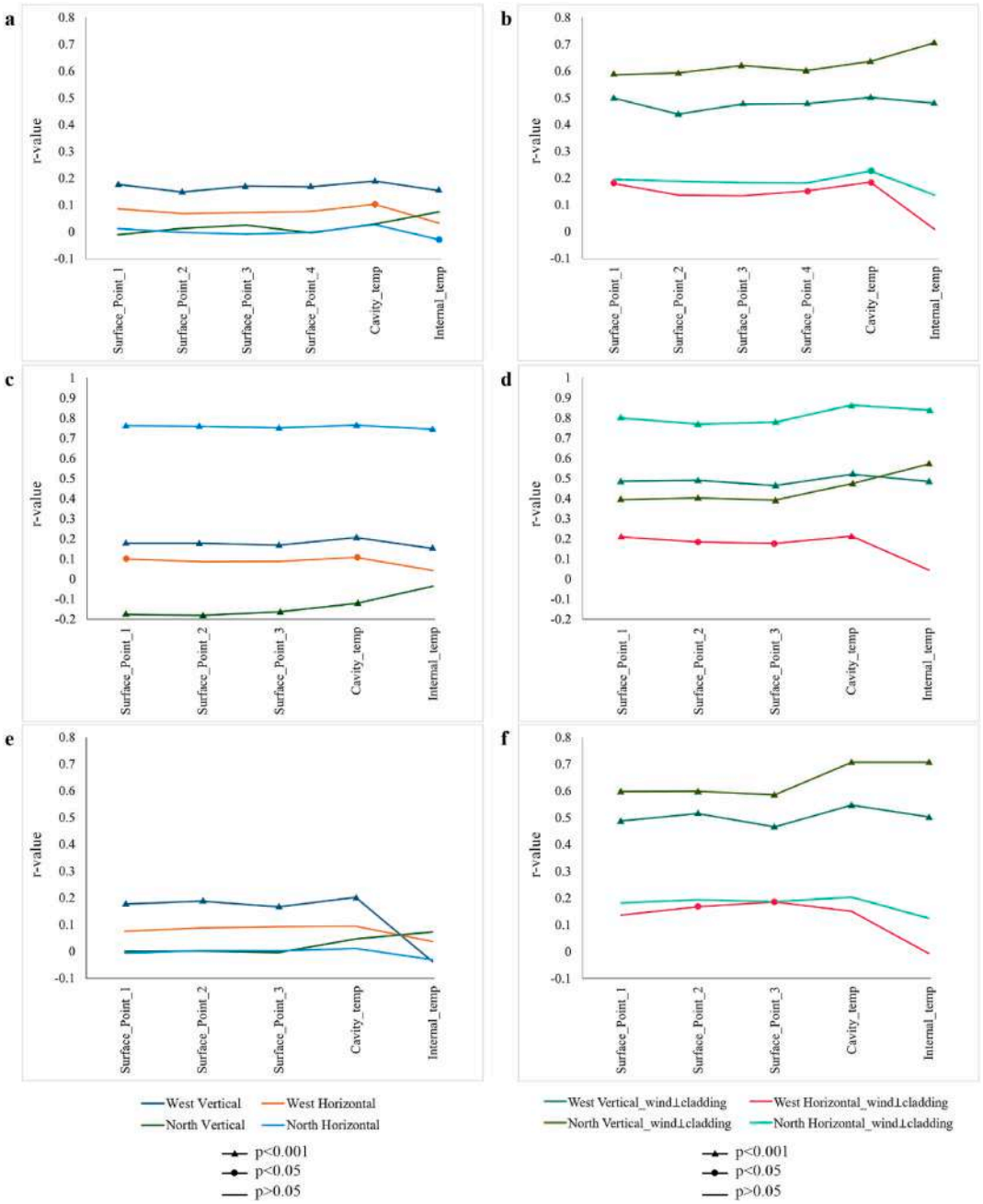

Fig. 14. Correlation between SS-Standing Seam (a–b), CR-Corrugated (c–d), and IL-Interlocking (e–f) profiles with wind speed: unfiltered data (a, c, e) and perpendicular wind only (b, d, f).

understanding how profile geometry, orientation, and rib configuration impact thermal behaviour. These results form the basis for ongoing work where the data is used to calibrate a simulation model. Once validated, the model can be scaled to represent realistic buildings more accurately. As such, the findings should be interpreted as a controlled comparison rather than a direct reflection of full-scale performance.

4.2. Surface temperature of each profile

Previous studies have explored the concept of self-shading, where components of the façade provide shading to reduce temperatures in the shadowed areas [19]. Although research on opaque surfaces and the use of high-conductance materials remains limited, the findings of this study suggest that self-shading principles can be effectively applied to steel cladding systems. The findings

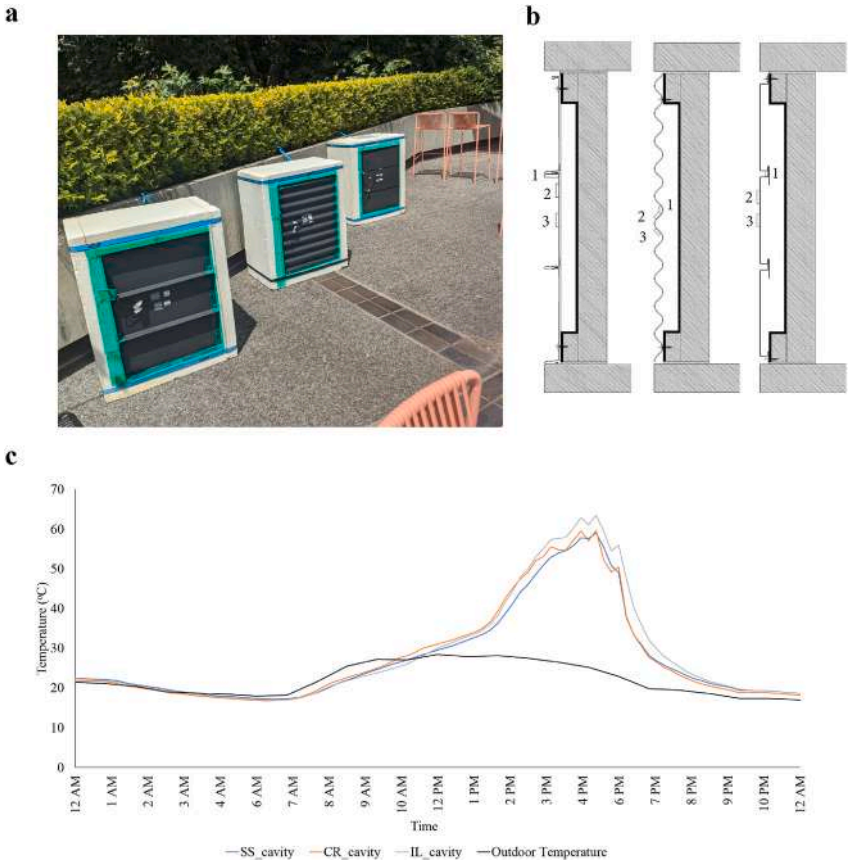

Fig. 15. (a) Physical setup with grill mask tape applied around the perimeter of the steel cladding; (b) section view indicating the surface temperature probe locations; (c) representative cavity temperature comparison between the three setups on 12 November.

Table 7
Surface temperature measurement with airflow restricted.

Cladding type	Measurement points pair	Min Temp Difference (°C)	Max Temp Difference (°C)	Avg Temp Difference (°C)
SS (Standing seam)	Point1 - Point2	0.00 (occurred during the night)	−9.64	−0.24
	Point1- Point3		−10.15	−0.25
	Point2- Point3		−0.95	−0.23
CR (Corrugated)	Point1 - Point2	0.00 (occurred during the night)	+3.42	+0.26
	Point1- Point3		+4.56	−0.19
	Point2- Point3		+2.23	−0.32
IL (Interlocking)	Point1 - Point2	0.00 (occurred during the night)	−2.70	−0.26
	Point1- Point3		+13.81	+0.33
	Point2- Point3		+16.16	+0.51

+ Indicates the first profile has a higher temperature, - Indicates the first profile has a lower temperature.

demonstrate that rib positioning and orientation significantly influenced surface temperature dynamics across different profiles.

The SS profile highlights the role of self-shading, with ribs and nearby surfaces consistently showing lower temperatures (by over 7 °C in both west-vertical and north-horizontal orientations). This underscores the capacity of self-shading to mitigate heat accumulation despite the high thermal conductivity of steel cladding.

The CR profile exhibits pronounced thermal behaviour linked to its valley and crest design. The surface temperature of the valley showed consistently higher temperatures during low sun angles, indicating heat entrapment in valley regions. In contrast, the surface temperature on the crest shows relatively lower but still variable temperatures throughout the day.

Practical implications suggest that the valley areas may experience higher thermal loads, particularly in afternoon sun conditions. This could be mitigated by incorporating reflective or insulating materials in the valley sections. A further study could focus on how corrugated designs might be modified for example, by adjusting rib spacing, height, or angle to increase self-shading effects. This could subsequently reduce heat transfer to the cavity by limiting direct solar exposure through enhanced shading, particularly in valley regions.

The findings for the IL profile reveal that the surface temperature of the recessed areas, similar to the valleys in corrugated profiles, was higher than that of the crest, despite being partially shaded. This outcome may be attributed to the combined effects of reflected shortwave radiation from adjacent surfaces and reduced convective heat loss within the recess. Although recessed areas are partially shaded, their geometry can trap heat by limiting air movement and allowing solar radiation to bounce within the cavity, thereby raising the local surface temperature. Previous studies have highlighted the role of external longwave radiation in building energy performance, particularly as surface temperature variations increase radiative exchanges between surfaces [62,63]. Moreover, recent research suggests that in dense or complex environments, longwave radiation emitted from surrounding surfaces may contribute more significantly to radiative exchange than sky radiation, reducing the sensitivity of such models to sky view factor (SVF) inputs [64]. This suggests that managing reflected radiation in recessed areas is essential for optimising thermal performance. Further studies, such as those focusing on re-radiation in similar materials, could provide deeper insights into this effect.

Furthermore, in relation to the colour of the cladding and its solar absorptivity, the use of dark grey steel profiles ($\alpha = 0.73$) was intended to simulate a worst-case scenario. Although this study did not explicitly examine lighter or reflective coatings, previous research suggests that coating colour and reflectivity can significantly influence thermal performance. Joudi et al. [65] indicated that high total solar reflectance (TSR) exterior claddings can reduce cooling demand, while Hu et al. [66] demonstrated through outdoor exposure experiments that high-reflectance colours with optimised spectral selectivity in the 600–800 nm and 1200–1400 nm bands can effectively lower surface temperatures and indoor heat gain. These findings suggest that, even with self-shading features, the choice of coating colour or reflectivity could further modulate cavity and internal temperatures, with high-reflectance coatings potentially amplifying the cooling effect provided by self-shading elements. The results of this study, therefore, should be interpreted within the context of the selected dark grey profiles, with the understanding that other coatings could modify the absolute thermal performance but are unlikely to change the relative trends observed between different cladding profiles.

4.3. Airflow in the experiment

Understanding the role of airflow in steel cladding systems is essential for evaluating their thermal performance. Airflow within the cavity of the cladding system plays a significant role in heat transfer, which enhances convective heat transfer. In the absence of wind, buoyancy-driven airflow is the dominant mechanism for air movement, caused by solar radiation heating the cladding surface and subsequently warming the air inside the cavity [67]. When no inlet or outlet is provided in a façade made of high thermal conductivity materials, the cavity temperature tends to rise above the ambient temperature [68].

When wind is present, it generates forced convection, which becomes the dominant factor in the airflow within the cavity [67,69]. As wind interacts with the cladding surface, it enhances convective heat transfer, reducing the surface and cavity temperatures. This effect is particularly notable when the wind direction aligns with the cladding orientation, as it leads to a higher efficiency of heat dissipation. Studies have demonstrated that wind speed and direction significantly affect the convective heat transfer inside the cavity [70–72]. The experimental results support these findings, showing that the alignment of wind direction with the cladding orientation leads to moderate correlations between wind speed and temperature variations within the cavity. This pattern was consistent across the various cladding profiles tested in the study, further confirming the influence of wind in promoting forced convection and cooling the steel cladding system.

The recessed part could create turbulence that enhances mixing between the flow at the wall and the central fluid flow, creating thermal mixing between the flow near the wall and the central fluid [73]. Turbulent mixing in such cavities increases heat transfer by continuously transporting warmer air away from the surface and replacing it with cooler air, reducing thermal stratification and improving overall cavity cooling [56]. Another study, although applied on a larger scale such as balconies, indicates that the recessed part of the balcony affects the airflow by creating larger recirculation zones, which leads to an increase in wind speed on windward balcony spaces. For instance, increasing the depth of balconies from 1 m to 4 m results in a 75.6 % increase in the area-averaged wind speed (Kavg). Moreover, the increased depth reduces the façade-averaged pressure coefficient (Cp,avg) on the windward façade, from 0.660 to 0.609, indicating a decrease in negative wind pressure [74]. This concept can help explain airflow patterns around cladding profiles with varying depths.

In the case of steel cladding, the depth of the balcony is analogous to the depth of the ribs. Just as deeper balconies alter airflow on the external façade, deeper ribs on the cladding can disrupt airflow, creating localised pressure changes. These changes in pressure can lead to lower negative pressures behind the cladding, which may improve heat transfer by promoting better air circulation and reducing thermal buildup in the cavity. Furthermore, increased airflow around the ribs can enhance convective heat transfer, helping to regulate temperature more efficiently and reducing the thermal load on the cladding. As observed in studies, variations in pressure coefficients, driven by factors such as wind direction and geometry, have significant impacts on airflow rates, influencing natural ventilation and convective cooling within cavities [75]. The ability of the cladding to harness such airflow, especially in deeper configurations, can thus play a critical role in improving thermal performance.

Importantly, cavity sealing significantly modifies these effects. In sealed conditions, the standing seam profile with a narrow 42 mm cavity exhibits lower temperatures compared to wider cavities, such as corrugated or interlocking profiles, due to reduced space for thermal stratification. From a heat transfer perspective, reducing cavity depth decreases the characteristic length in the Rayleigh number, thereby lowering Ra and suppressing buoyancy-driven convection [76,77]. At low Ra, heat transfer becomes conduction-dominated, so convection remains weak. This helps explain why standing seam and corrugated profiles with self-shading features perform better than the interlocking profile, which lacks ribs. In contrast, wider sealed cavities, such as interlocking profiles, may support stronger convection [58]. However, without adequate airflow, these cavities can experience thermal stratification, where warmer air accumulates at the top, potentially trapping heat and increasing thermal load. Conversely, in unsealed conditions, narrow

cavities such as the standing seam can perform worse than wider cavities because limited airflow restricts convective heat removal, whereas wider cavities allow natural or wind-driven convection through gaps and outlets, enhancing cooling. The performance of interlocking and corrugated profiles under unsealed conditions is further influenced by rib orientation, with horizontal ribs favouring airflow paths that enhance cooling, while vertical ribs can guide airflow differently, sometimes improving heat dissipation in interlocking profiles.

These findings are consistent with previous studies that highlight the critical role of wind in improving cooling efficiency and heat dissipation from surfaces [78]. Higher wind speeds enhance the cooling effect, while low wind speeds reduce cooling efficiency by allowing heat to accumulate. Additionally, the current experiment aligns with research indicating that wind conditions affect cavity air velocity, which in turn reduces thermal resistance and improves the overall thermal performance of the cladding system [49].

5. Limitations of the experiment

To limit the scope of this paper, the experiment was conducted solely on opaque surfaces, focusing on the thermal performance of the cladding itself. This serves as the basis for further studies aimed at calibrating and validating the results. The experiment employed a passive, solar-only setup, which allows capturing the thermal behaviour of steel cladding under realistic environmental conditions, including variations in sun exposure, wind, and ambient temperature. While this approach reflects true outdoor conditions, the variability of the microclimate introduces uncertainties that are difficult to control, representing a limitation of the method.

Additionally, this analysis focused on isolating the contribution of the steel cladding itself, without introducing additional variables such as window glazing, which typically dominates solar heat gain [79]. The results show that internal and cavity temperatures vary depending on the cladding profile shape. These findings highlight the importance of cladding geometry for thermal performance and provide a foundation for future studies exploring more complex building configurations.

The experiment was conducted at the University of Adelaide's Waite Campus, located in the southern part of the CBD. This location was chosen to minimise human interference and maximise exposure to solar radiation. However, the sloped terrain and natural surroundings may not be representative of the conditions in more urban environments. Despite taking precautions, such as using star droppers and barrier mesh, the testing site was subject to potential disturbances from wildlife. These disturbances could have affected the experimental setup and data integrity momentarily, as wildlife might interact with or disrupt the assembly. The experimental setup, which included lightweight polystyrene boxes, was also susceptible to wind. Although measures were taken to secure the boxes by tying them to wooden pallets, there were instances when the boxes were pushed by the wind. This required the researcher to repeatedly fix the setup, which meant that data could not be used when the experiment was down. Furthermore, while the construction was carried out with as much accuracy as possible, unavoidable imperfections in the construction can impact the thermal performance of the experiment setup. Previous research on Hot Boxes by Barbaresi et al. [33], for example, has shown that thermal bridging can occur in experimental setups due to imperfect construction, which needs to be kept in mind when validating the results. Additionally, the absence of a fan in the experimental setup means that natural temperature distribution inside the boxes was observed, which could potentially affect temperature homogeneity. While this design avoids introducing forced convection, which could alter the natural thermal behaviour, it also means that the temperature distribution may not fully represent a uniform internal temperature.

To examine the potential influence of uncontrolled convective airflow within the cavity, a comparison was made between unsealed and sealed conditions using perforated grill mask tape. While this approach helped reduce air leakage and allowed observation of its effect on cavity temperatures, exact airflow rates were not measured due to the small size of the 4 cm cavity, which limits the feasibility of conventional airflow measurement techniques. Future studies incorporating direct airflow measurements within the cavity could provide more precise insights into the influence of convective currents on thermal performance.

Furthermore, the thermal transfer tape used to attach the probes may introduce some errors due to differences in its thermal and radiative properties compared to the steel cladding. While the tape ensures good thermal contact, its solar absorptance and emissivity are not provided by the manufacturer, and therefore its thermal properties may not match those of the steel cladding (solar absorptance of 0.73 and emissivity of 0.87). However, since the goal is to compare temperature differences between the probe locations, this potential error is considered acceptable for the experiment.

6. Conclusion

This paper presents experiments designed to assess the thermal performance of three steel cladding profiles under varying orientations and rib directions. In hot climates, solar heat gain is primarily driven by building glazing. However, this study explores how opaque steel cladding profiles, with their self-shading features, can help reduce heat gain through the façade. The findings reveal that orientation, profile shape, and airflow significantly influence the surface of the envelope, heat transfer and heat gain in the internal space.

A comparison between the three profiles showed distinct thermal behaviours. The SS (Standing Seam) profile consistently exhibited the highest cavity temperatures during the day, particularly when ribs were oriented horizontally and westward, with temperature differences exceeding 20 °C compared to the CR (Corrugated) profile. CR profile, while generally cooler during the day, tended to retain more heat overnight, resulting in slightly higher temperatures than the other profiles during nighttime. In contrast, the IL (Interlocking) profile consistently showed the lowest cavity temperatures throughout the day, especially when oriented northward, with temperature differences widening to more than 15 °C by late afternoon. These observations highlight the significant influence of profile geometry on both daytime heat gain and nighttime cooling.

The combined effect of these factors can lead to a notable reduction in both cavity and internal temperatures. For instance, the

traditional corrugated profile demonstrated reduced heat gain to the internal zone, particularly when oriented horizontally. While this profile is typically used vertically in practice to prevent rainwater and debris accumulation, the results suggest that horizontal corrugation may be more effective in minimising heat gain. This indicates that an improvement of corrugation design, optimised for heat reduction and integrated with a cavity ventilation approach that promotes buoyancy-driven or wind-assisted airflow, could mitigate traditional concerns while improving thermal efficiency. Additionally, the reduced heat gain extends to internal temperatures, implying that this strategy could complement other façade measures, such as improved insulation.

The self-shading effect was also evident across the steel profiles' surface temperatures, with areas near ribs consistently showing lower surface temperatures, by over 7 °C in some cases. Additionally, inward protrusion, such as valleys and recesses, is shown to have influenced thermal behaviour by increasing exposure to reflected shortwave and longwave radiation from adjacent surfaces, contributing to localised heat accumulation.

Furthermore, airflow within the cavity, influenced by external wind and convection, is likely to be a factor in the thermal performance of all profiles. The results showed stronger correlations between wind speed and both cavity and internal temperatures when the profiles were oriented in the direction of the wind. The correlation coefficients for cavity and internal temperatures increase to approximately 0.4 and 0.3, respectively ($p < 0.001$), nearly double the values when wind direction was not considered. However, the correlation between wind speed and internal temperature was generally lower by 0.01–0.05 compared to cavity temperature, due to the insulative properties of expanded polystyrene, which reduced the effect of convection through the wind. When a subsequent experiment was conducted to minimise the effect of airflow, the results indicated that the profile, which lacks the shaded area provided by protruding ribs, namely the Interlocking profile, exhibited the highest cavity temperature. This suggests that when airflow was no longer a dominant factor, the shaded area of the steel cladding/sheet became the primary determinant of heat gain differences.

Based on these findings, the following design recommendations can be made to guide further research or design iterations.

- Profile selection: Profiles with protruded ribs generally reduce cavity and internal temperatures more effectively, demonstrating a stronger self-shading effect than profiles with flatter or less articulated surfaces. In this study, corrugated profiles showed this advantage more clearly than standing seam and interlocking profiles.
- Cavity gap: The width of the cavity influences convective behaviour. Providing an air cavity of at least 40 mm behind the cladding helps improve airflow and reduce heat build-up in the wall assembly.
- Rib direction: Horizontal rib direction enhances the self-shading effect for both north and west-facing facades and can improve heat dissipation by promoting airflow under natural ventilation conditions, enhancing thermal performance.

The study highlights several areas for further research. While the results indicate that self-shading from profile morphologies can reduce heat gain, they also suggest that the wind may play a role in this process. However, the findings do not establish a causal relationship between wind and cavity and internal temperatures. Therefore, a more detailed analysis is needed to understand the effects of wind speed, airflow within the cavity, and wind direction on cladding temperature and heat transfer to both the cavity and the interior. This study also only focused on steel sheet cladding with profiles that are commonly used in Adelaide's buildings, with specific surface properties (particularly solar absorptivity of 0.73). Future studies should explore different surface characteristics and investigate how varying cladding designs, such as rib and recess shapes and orientations, affect the thermal performance of the cladding and buildings with such claddings. Such studies will offer further valuable insights into strategies for enhancing energy efficiency and thermal comfort in buildings.

CRediT authorship contribution statement

Ricardo Lionar: Writing – review & editing, Writing – original draft, Visualization, Methodology, Investigation, Formal analysis, Data curation, Conceptualization. **David Kroll:** Writing – review & editing, Supervision, Methodology, Formal analysis. **Veronica Soebarto:** Writing – review & editing, Supervision, Methodology, Investigation, Formal analysis. **Ehsan Sharifi:** Writing – review & editing, Validation, Supervision, Resources, Methodology, Formal analysis. **Marina Aburas:** Writing – review & editing, Supervision, Resources, Funding acquisition.

Declaration of competing interest

The authors declare the following financial interests/personal relationships which may be considered as potential competing interests: Ricardo Lionar reports financial support was provided by Bluescope Steel Limited. If there are other authors, they declare that they have no known competing financial interests or personal relationships that could have appeared to influence the work reported in this paper.

Acknowledgments

This research is funded through The University of Adelaide Industry PhD scholarship with Bluescope Building Components. We also extend our gratitude to Bluescope Building Components for the generous provision of materials and funding.

Data availability

Data will be made available on request.

References

[1] H. Heritage South Australia Department for Environment, A. Aboriginal, Early Roofing and Roof Materials in South Australia, 1999.
[2] D.M. Howell, Metal cladding for roofs and walls — will it meet your needs? Constr. Build. Mater. 2 (1) (1988) 10–15.
[3] R. Grand View, Cladding Market Size, Share & Trends Analysis Report by Product (Fiber Cement, Composite Material, Terracotta, Ceramics), by Application (Residential, Commercial, Industrial), by Region, and Segment Forecasts, 2023, 2024 - 2030.
[4] I. Australian Steel, Steel Wall Cladding 2024.
[5] S. Gupta, Global Metal Cladding Market Overview, Market Research Future, 2025.
[6] G. Athmarajah, M. Mahendran, A. Ariyanayagam, Numerical modelling and design of cold-formed steel battens subject to pull-out failures under bushfire conditions, Eng. Struct. 319 (2024) 118776.
[7] K. Roy, Wind-uplift capacity of cold-formed steel interlocking claddings-experimental and numerical investigations, J. Build. Eng. 63 (2023).
[8] H. Hofmeyer, S.W.A. Geers, H.H. Snijder, B.W. Schafer, The direct strength Method for first generation trapezoidal steel sheeting under interior one flange and interior two flange web crippling, Thin-Walled Struct. 180 (2022) 109795.
[9] A.C. Lovisa, D.J. Henderson, J.D. Ginger, G. Walker, Characterising fatigue macrocrack initiation in profiled steel roof cladding, Eng. Struct. 125 (2016) 364–373.
[10] D. Mahaarachchi, Behaviour and Design of Profiled Steel Cladding Systems Subject to pull-through Failures, Queensland University of Technology, 2003.
[11] I. British Standards, BS EN 1993-1-3:2024 Eurocode 3 - Design of Steel Structures. Cold-formed Members and Sheeting, 2024.
[12] R. Fayaz, B.M. Kari, Comparison of energy conservation building codes of Iran, Turkey, Germany, China, ISO 9164 and EN 832, Appl. Energy 86 (10) (2009) 1949–1955.
[13] F. Taha, N. El Mahallawy, M. Shoeib, A study of sol gel process parameters on CoCuMnOx selective coating characteristics, Mater. Res. Express 7 (2) (2020).
[14] V. Amrutha, A. Dan, J. Gabirondo-Lopez, T. Echaniz, R. Fuente, H.C. Barshilia, G.A. Lopez, In situ high-temperature emissivity measurements of heat-treated, silicon coated stainless steel for solar thermal applications, Sol. Energy Mater. Sol. Cell. 279 (2025).
[15] J. Min, W. Yuan, Y. Chen, Y. Lan, M. Yan, H. Liu, X. Cheng, L. Dai, Preparation and thermal stability of AlMoON based solar selective absorption coating, J. Wuhan Univ. Technol.-Materials Sci. Ed. 39 (4) (2024) 854–862.
[16] P. Čanda, P. Kopecký, Thermal performance of roofs suitable for developing countries in tropical climate, J. Phys.: Conf. Ser. 2069 (1) (2021) 012202.
[17] X. Wang, C. Kendrick, R. Ogden, J. Maxted, Dynamic thermal simulation of a retail shed with solar reflective coatings, Appl. Therm. Eng. 28 (8) (2008) 1066–1073.
[18] R. Levinson, H. Akbari, J.C. Reilly, Cooler tile-roofed buildings with near-infrared-reflective non-white coatings, Build. Environ. 42 (7) (2007) 2591–2605.
[19] R. Lionar, D. Kroll, V. Soebarto, E. Sharifi, M. Aburas, A review of research on self-shading façades in warm climates, Energy Build. 314 (2024) 114203.
[20] H. Tang, J. Peng, H. Peng, Y. Yang, Q. Gao, L. Xiao, H. Li, L. Zheng, Z. Chen, Z. Yang, Test and theoretical investigations on flexural behavior of high-performance H-Shaped steel beam with local corrosion in pure bending Zone, Steel Res. Int. 96 (7) (2025) 2400640.
[21] S. Xiong, N. Yang, H. Guan, G. Shi, M. Luo, Y. Deguchi, M. Cui, Combination of plasma acoustic emission signal and laser-induced breakdown spectroscopy for accurate classification of steel, Anal. Chim. Acta 1336 (2025) 343496.
[22] B. Chen, F. Qiu, L. Xia, L. Xu, J. Jin, G. Gou, In situ ultrasonic characterization of hydrogen damage evolution in X80 pipeline steel, Materials 17 (23) (2024) 5891.
[23] D. Ren, C. Wang, X. Wei, Y. Zhang, S. Han, W. Xu, Harmonizing physical and deep learning modeling: a computationally efficient and interpretable approach for property prediction, Scr. Mater. 255 (2025) 116350.
[24] Y. Li, D.S. Martín, J. Wang, C. Wang, W. Xu, A review of the thermal stability of metastable austenite in steels: martensite formation, J. Mater. Sci. Technol. 91 (2021) 200–214.
[25] C. Shen, C. Wang, X. Wei, Y. Li, S. van der Zwaag, W. Xu, Physical metallurgy-guided machine learning and artificial intelligent design of ultrahigh-strength stainless steel, Acta Mater. 179 (2019) 201–214.
[26] A. Soltani, E. Sharifi, Daily variation of urban heat island effect and its correlations to urban greenery: a case study of Adelaide, Frontiers of Architectural Research 6 (4) (2017) 529–538.
[27] F.M. Selten, R. Bintanja, R. Vautard, B.J.J.M. van den Hurk, Future continental summer warming constrained by the present-day seasonal cycle of surface hydrology, Sci. Rep. 10 (1) (2020) 4721.
[28] J. Falk, K. Sandin, Ventilated rainscreen cladding: measurements of cavity air velocities, estimation of air change rates and evaluation of driving forces, Build. Environ. 59 (2013) 164–176.
[29] C. Sanjuan, M.J. Suárez, M. González, J. Pistono, E. Blanco, Energy performance of an open-joint ventilated façade compared with a conventional sealed cavity façade, Sol. Energy 85 (9) (2011) 1851–1863.
[30] S. Hendawitharana, A. Ariyanayagam, M. Mahendran, Predicting the behaviour of external steel walls under bushfire radiant heat conditions, Fire Saf. J. 141 (2023) 103888.
[31] S. Golder, R. Narayanan, M.R. Hossain, M.R. Islam, Experimental and CFD investigation on the application for Aerogel insulation in buildings, Energies 14 (11) (2021) 3310.
[32] G. Salvalai, M.M. Sesana, Experimental analysis of different insulated façade technologies in summer condition, Journal of Green Building 14 (4) (2019) 77–91.
[33] A. Barbaresi, M. Bovo, E. Santolini, L. Barbaresi, D. Torreggiani, P. Tassinari, Development of a low-cost movable hot box for a preliminary definition of the thermal conductance of building envelopes, Build. Environ. 180 (2020) 107034.
[34] B. Peters, A. Sharag-Eldin, B. Callaghan, Development of a Simple Hot Box to Determine the Thermal Characteristics of a three-dimensional Printed Bricks, 2017.
[35] J.Y. Chang, Y.D. Kuan, C.C. Lan, H.J. Li, Y.K. Hsu, C.Y. Chen, E.T. Shen, K.Y. Lin, Discussion of the energy-saving benefits of heat insulating coating for building windows. MATEC Web of Conferences, 2016.
[36] B. Australian Building Codes, National Construction Code, (2022).
[37] A. Joudi, H. Svedung, C. Bales, M. Rönnelid, Highly reflective coatings for interior and exterior steel cladding and the energy efficiency of buildings, Appl. Energy 88 (12) (2011) 4655–4666.
[38] J.M. Lirola, E. Castañeda, B. Lauret, M. Khayet, A review on experimental research using scale models for buildings: application and methodologies, Energy Build. 142 (2017) 72–110.
[39] D. Etheridge, Scale Modelling, Natural Ventilation of Buildings, John Wiley and Sons, Ltd, 2011.
[40] N. Khan, Y. Su, S.B. Riffat, A review on wind driven ventilation techniques, Energy Build. 40 (8) (2008) 1586–1604.
[41] A.M. Bazzi, Z. Klein, M. Sweeney, K.P. Kroeger, P.S. Shenoy, P.T. Krein, Solid-state solar simulator, IEEE Trans. Ind. Appl. 48 (4) (2012) 1195–1202.
[42] S. Liu, G. Zhang, G. Sun, L. Wang, Y. Gao, Design of an optical system for a solar simulator with high collimation degree and high irradiance, J. Opt. Technol., JOT 84 (2) (2017) 117–121.
[43] C.A. Gueymard, The SMARTS spectral irradiance model after 25 years: new developments and validation of reference spectra, Sol. Energy 187 (2019) 233–253.
[44] J. Jin, Y. Hao, H. Jin, A universal solar simulator for focused and quasi-collimated beams, Appl. Energy 235 (2019) 1266–1276.
[45] S. Kim, J. Seo, H. Jeong, J. Kim, In situ measurement of the heat loss coefficient of thermal bridges in a building envelope, Energy Build. 256 (2022) 111627.

[46] L. Iskandar, C. Faubel, A. Martinez-Molina, S. Toker Beeson, Quantification of inherent energy efficient features in historic buildings under hot and humid conditions, Energy Build. 319 (2024) 114546.
[47] J. Rothleder, K. Herken, Specifications and Tolerances, for Reference Standards and Field Standard Weights and Measures, U.S. Department of Commerce, 1996.
[48] D. Cui, G. Liang, J. Hang, Z. Yang, Z. Huang, C.M. Mak, Effects of envelope features on building surface temperature and ventilation performance in 2D street canyons, Urban Clim. 56 (2024).
[49] G. Mammadova, A. Sharifov, S. Akbarova, Experimental study of air cavity thermal performance of opaque ventilated facades under extreme wind conditions: case study Baku, Inf. Construcción 73 (561) (2021) e376-e376.
[50] O. McCay, R. Nimmagadda, S.M. Ali, T. Persoons, A parametric design study of natural-convection-cooled heat sinks, Fluid 8 (8) (2023) 234.
[51] B. Yazicioğlu, H. Yüncü, Optimum fin spacing of rectangular fins on a vertical base in free convection heat transfer, Heat Mass Tran. 44 (1) (2007) 11–21.
[52] U.S.D.o. Energy, Principles of heating and cooling, Energy.gov.
[53] I. Luginbuehl, B. Bissonnette, Chapter 25 - thermal regulation, in: C.J. Coté, J. Lerman, I.D. Todres (Eds.), A Practice of Anesthesia for Infants and Children, fourth ed., W.B. Saunders, Philadelphia, 2009, pp. 557–567.
[54] S. Gao, R. Ooka, W. Oh, Formulation of human body heat transfer coefficient under various ambient temperature, air speed and direction based on experiments and CFD, Build. Environ. 160 (2019) 106168.
[55] A. Sadeghianjahromi, S. Kheradmand, H. Nemati, J.-S. Liaw, C.-C. Wang, Compound heat transfer enhancement of Wavy fin-and-tube heat exchangers through boundary layer restarting and swirled flow, Energies 11 (8) (2018) 1959.
[56] J. Xamán, G. Álvarez, L. Lira, C. Estrada, Numerical study of heat transfer by laminar and turbulent natural convection in tall cavities of façade elements, Energy Build. 37 (7) (2005) 787–794.
[57] J. Hærvig, H. Sørensen, Natural convective flow and heat transfer on unconfined isothermal zigzag-shaped ribbed vertical surfaces, Int. Commun. Heat Mass Tran. 119 (2020) 104982.
[58] G.M. Girma, F. Tariku, Experimental investigation of cavity air gap depth for enhanced thermal performance of ventilated rain-screen walls, Build. Environ. 194 (2021) 107710.
[59] M. Ciampi, F. Leccese, G. Tuoni, Ventilated facades energy performance in summer cooling of buildings, Sol. Energy 75 (6) (2003) 491–502.
[60] C. Balocco, A simple model to study ventilated facades energy performance, Energy Build. 34 (5) (2002) 469–475.
[61] R.J. Zupan, D.T. Clifford, R.V. Beblo, J.C. Brigham, Design, prototyping, and evaluation of a concept for a shape-changing smart material building surface tile, Smart Mater. Struct. 29 (11) (2020).
[62] R. Evins, V. Dorer, J. Carmeliet, Simulating external longwave radiation exchange for buildings, Energy Build. 75 (2014) 472–482.
[63] X. Xie, Z. Luo, S. Grimmond, T. Sun, W. Morrison, Impact of inter-building longwave radiative exchanges on building energy performance and indoor overheating, Build. Environ. 209 (2022) 108628.
[64] C. Zhao, L. Zhang, Y. Zhang, Exploring the effect of longwave radiation exchange on the energy balance of building façades in subtropical regions, Build. Environ. 233 (2023) 110096.
[65] A. Joudi, M. Cehlin, H. Svedung, M. Rönnelid, B. Moshfegh, Numerical and experimental investigation of the influence of infrared reflective interior surfaces on building temperature distributions, Indoor Built Environ. 26 (3) (2017) 355–367.
[66] C. Hu, G. Zhang, X. Meng, F. He, Influence of color reflectance on the thermal performance of building facades: a factor model-based detective analysis, Case Stud. Therm. Eng. 67 (2025) 105793.
[67] A. Gagliano, F. Nocera, S. Aneli, Thermodynamic analysis of ventilated façades under different wind conditions in summer period, Energy Build. 122 (2016) 131–139.
[68] J. Balter, C. March, I. Ansuategui, C. Ganem, Air cavity performance in Opaque ventilated façades in accordance with the Spanish technical Building code, ACE - Archit. City Environ. 13 (2019) 211–232.
[69] S. Matour, V. Garcia-Hansen, S. Omrani, S. Hassanli, R. Drogemuller, Wind-driven ventilation of double skin façades with vertical openings: effects of opening configurations, Build. Environ. 196 (2021) 107804.
[70] S. Hassanli, K.C.S. Kwok, M. Zhao, Performance assessment of a special double skin façade system for wind energy harvesting and a case study, J. Wind Eng. Ind. Aerod. 175 (2018) 292–304.
[71] S. Hassanli, G. Hu, D.F. Fletcher, K.C.S. Kwok, Potential application of double skin façade incorporating aerodynamic modifications for wind energy harvesting, J. Wind Eng. Ind. Aerod. 174 (2018) 269–280.
[72] S. Flores Larsen, L. Rengifo, C. Filippín, Double skin glazed façades in sunny mediterranean climates, Energy Build. 102 (2015) 18–31.
[73] A. Azman, A. Mukhtar, M.Z. Yusoff, P. Gunnasegaran, N. Khai Ching, A.S.H. Md Yasir, Numerical investigation of flow characteristics and heat transfer efficiency in sawtooth corrugated pipes with Al2O3-CuO/Water hybrid nanofluid, Results Phys. 53 (2023) 106974.
[74] X. Zheng, H. Montazeri, B. Blocken, CFD analysis of the impact of geometrical characteristics of building balconies on near-façade wind flow and surface pressure, Build. Environ. 200 (2021) 107904.
[75] R. Ramponi, A. Angelotti, B. Blocken, Energy saving potential of night ventilation: sensitivity to pressure coefficients for different European climates, Appl. Energy 123 (2014) 185–195.
[76] A. Kangni, R. Ben Yedder, E. Bilgen, Natural convection and conduction in enclosures with multiple vertical partitions, Int. J. Heat Mass Tran. 34 (11) (1991) 2819–2825.
[77] S. Lorente, M. Petit, R. Javelas, Simplified analytical model for thermal transfer in vertical hollow brick, Energy Build. 24 (2) (1996) 95–103.
[78] Arup, Bluescope Microclimate Thermal Study, 2017.
[79] W. Liao, C. Wen, Y. Luo, J. Peng, N. Li, Influence of different building transparent envelopes on energy consumption and thermal environment of radiant ceiling heating and cooling systems, Energy Build. 255 (2022) 111702.